Bio-Design and Manufacturing (2025) 8:1080–1102
https://doi.org/10.1631/bdm.2400389

REVIEW

Design of linear pneumatic artificial muscles guided by biomechanics of human skeletal muscle for wearable application: a review

Zhuo Ma[1] · Jianbin Liu[1] · Haitao Liu[1] · Tian Huang[1]

Received: 25 September 2024 / Accepted: 23 January 2025 / Published online: 27 October 2025

Abstract

Pneumatic artificial muscles (PAMs) can generate multimodal movements, e.g., linear contraction/extension, spiral torsion, and bending motions. Among these motions, contraction and extension movements can be achieved using linear PAMs (LPAMs) designed to mimic human skeletal muscle. LPAMs have considerable potential for wearable applications and can be integrated into soft wearable robotic systems. Due to their inherent compliance, excellent human–robot interaction, safety, and low cost, LPAMs are considered potential alternatives as actuator components in the construction of wearable robots. This review presents a comprehensive overview of the bio-inspired design of LPAMs and their wearable applications. The biomechanics of human skeletal muscle, including anatomy, morphology, and biomechanical characterization, is analyzed to provide design inspirations for LPAMs and determine the assistance requirements of LPAM-based wearable robots. Herein, LPAMs are classified into four categories based on their structural shapes, including cylindrical-shaped muscles, flat-shaped muscles, fold-shaped muscles, and muscles with other shapes. In addition, this review provides an overview of the diverse physical interfaces utilized in wearable robots and presents a comparative analysis of the actuation characteristics of LPAMs and the assistance performance of LPAM-based wearable robots. This analysis was conducted in consideration of several key metrics, including the contraction ratio, maximum force, specific force, response frequency, assistive torque/bodyweight, and net metabolic cost. Finally, this review summarizes the ongoing challenges and future research directions.

✉ Jianbin Liu
jianbin_liu@tju.edu.cn

[1] Key Laboratory of Mechanism Theory and Equipment Design of Ministry of Education, Tianjin University, Tianjin 300072, China

Graphical abstract

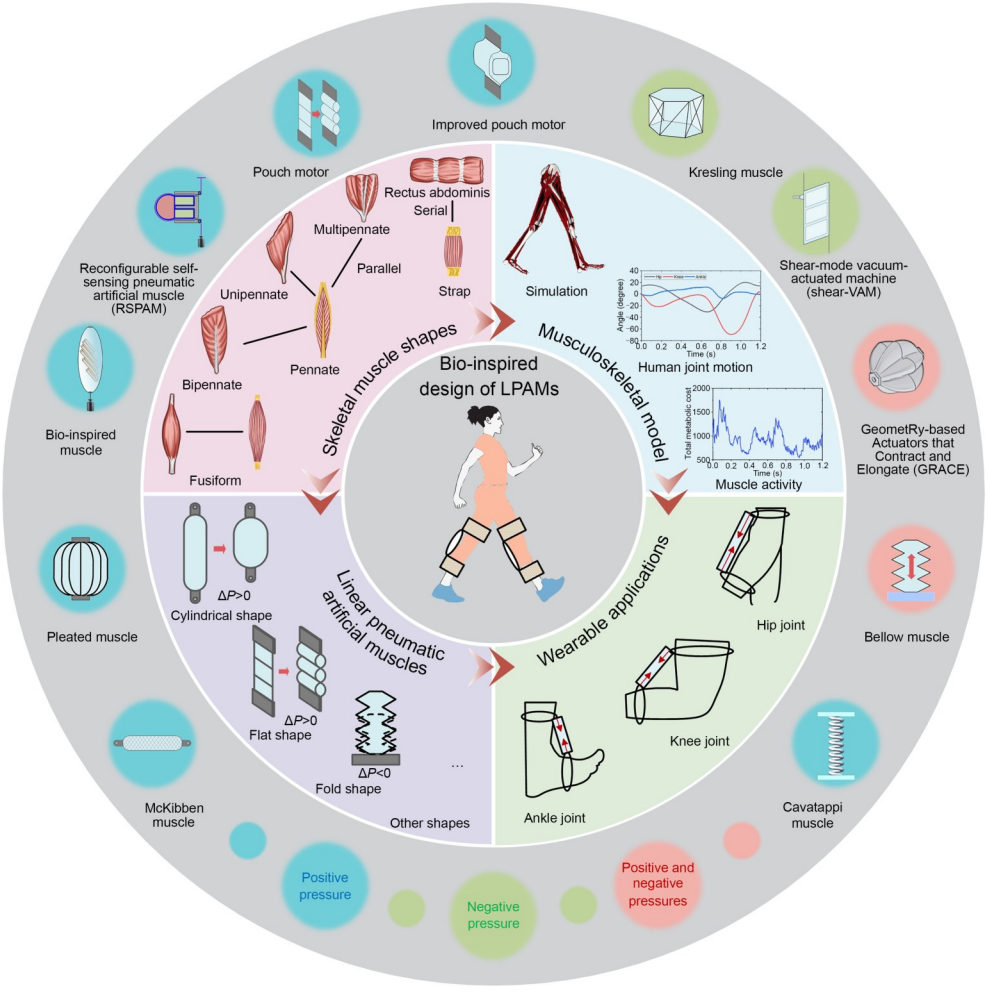

Keywords Pneumatic artificial muscle · Bio-inspired design · Biomechanics of human skeletal muscle · Wearable robots

1 Introduction

Soft wearable robotic systems can be used to assist individuals and patients with mild movement disorders in locomotion [1], and due to the rapid development of such systems, they are widely used in various fields, e.g., industrial assistance [2], rehabilitation training [3], and maintaining human postures [4]. Recently, soft wearable robotic systems have advanced because of existing technologies such as rigid exoskeletons and significant progress in wearable flexible electronics based on soft functional materials [5, 6]. A key feature of soft wearable robotic systems is the use of bio-inspired actuators that mimic the linear contraction of human skeletal muscle, which allows these systems to provide an assistive force parallel with the human body. The most used bio-inspired actuator is the pneumatic artificial muscle (PAM) [7], which is favored for its simple structure [8], excellent flexibility [9], rapid fabrication [10], and low cost [11].

The PAM consists of an inner bladder made of soft-film materials, an outer constricted fabric layer, and a small pipe joint [12]. The initial design objective of the PAM is to realize linear contraction, which is achieved by the McKibben muscle that is applied for wrist rehabilitation training [13]. Over the past decade, spiral torsion and bending motions have gradually emerged in the various actuators that are widely applied in soft grippers to perform industrial tasks, e.g., product grabbing and sorting in automated production [14]. In contrast to these soft actuators, a linear PAM (LPAM) is designed to mimic the contraction movement of human skeletal muscles. In this review, the term "PAM" is defined as pneumatic actuators containing a soft bladder

that can produce multimodal movements, and "LPAM" is defined as pneumatic actuators containing a soft bladder that can only generate linear movements, including contraction and extension. In other words, PAM represents a broader category that includes LPAM. This review focuses on the bio-inspired design methods of LPAMs guided by anatomical and biomechanical characteristics and their wearable applications in human lower limb joints.

The skeletal muscle is a crucial component of the human locomotor system that enables human movements, including walking, running, and squatting, which are completed by relying on antagonistic joints actuated by muscle contraction and extension. To mimic human skeletal muscles, scientists and engineers have developed numerous LPAMs whose actuation properties have been continuously improved. For example, a positive pressure-driven PAM, proposed by Feng et al. [15], exhibited an impressive contraction ratio of 92.9% and a remarkable strain rate of 1603.0% per second. This LPAM represents a nearly twofold increase in the contraction ratio compared with the McKibben muscle. In addition, a gusseted pouch motor that produces an output force of up to 526.5 N has been developed [16]. As the actuation properties of LPAMs approach those of skeletal muscle, the assistance requirements of human lower limb movements (e.g., level walking, rehabilitation training, sit-to-stand assistance, and uphill walking) can be satisfied by LPAMs worn on human bodies.

To date, many reviews focusing on different aspects of LPAMs have been published [17–19]. For example, Jamil et al. categorized LPAMs based on different materials, providing numerical comparisons of their capabilities and identifying future challenges in the field [20]. In addition, many reviews have investigated the static and dynamic modeling of LPAMs [21–23] and their application performance across various fields [22], and some reviews have also explored the design, manufacturing, sensing, control, and human–robot interaction methods of LPAMs [24]. These reviews offer valuable insights into the LPAMs; however, there is a lack of a comprehensive overview that specifically addresses bio-inspired designs guided by the anatomical and biomechanical characteristics of human skeletal muscles and summarizes the assistance performance of LPAM-based soft wearable robotic systems [25–27]. Thus, this review attempts to address this gap in the literature and serve as a useful reference for researchers interested in LPAM-based wearable robots or those looking to apply LPAMs in other research fields.

In this review, a comprehensive survey was conducted to summarize the existing research results on LPAMs that were fabricated for utilization in soft wearable robotic systems in the published articles, categorizing them by shape. Typically, LPAM designs are inspired by the anatomical and biomechanical characteristics of human skeletal muscle, where such LPAMs are driven by positive and negative pressures. Upon positive air pressure, the contraction force can be enhanced by increasing air pressure. In addition, the utilization of a negative pressure actuation mechanism enhances safety. By applying positive and negative pressures, LPAMs can exhibit both contraction and safety movement patterns.

This review surveys the physical interfaces that function as connection mechanisms between LPAMs and the human lower limbs. In addition, this review compares the results of the actuation characterizations of LPAMs and the assistance performance of LPAM-based wearable robots based on various critical metrics, including the contraction ratio, maximum force, specific force, response frequency, assistive torque/bodyweight, and net metabolic cost. The contraction ratio is a normalized metric that quantifies the output deformation of LPAMs, while the maximum force is a performance indicator of actuation. The specific force is defined as the output force per air pressure. Under the same conditions, the greater its value, the lower the air pressure required for LPAMs. Thus, low-power air pumps can be utilized to provide pneumatic energy for LPAMs with a high specific force, thereby reducing the weight of soft wearable robotic systems. The response frequency reflects the speed of changes in the output force, which determines whether the actuators satisfy the assistance requirements of the movements of the wearers. Using assistive torque/bodyweight to display the mechanical performance of LPAM-based wearable robots can avoid the impact of variation in body weight across different wearers. The net metabolic cost is used to determine the reduction rate of human physical energy consumption. Finally, this review discusses the persistent challenges and future directions for LPAM-based wearable robotic systems.

2 Human skeletal muscle

Muscle is a key component of the human body, accounting for 40% to 45% of the weight of the human body [28]. Based on the physiological characteristics and functions, muscles can be divided into three types, i.e., skeletal muscle, cardiac muscle, and smooth muscle, as shown in Fig. 1. Skeletal muscle, primarily located in the limbs and torso, constitutes the human locomotor system and is capable of voluntary contraction and extension. Note that cardiac muscle is only found in the heart, and it controls the heartbeat and blood circulation. Both the skeletal and cardiac muscles belong to striated muscle because their cytoplasm contains alternating light and dark bands [29]. In contrast, smooth muscle lacks striations and has a smooth and even surface, forming thin sheets. Smooth muscle is primarily distributed in internal organs, e.g., the stomach and intestine.

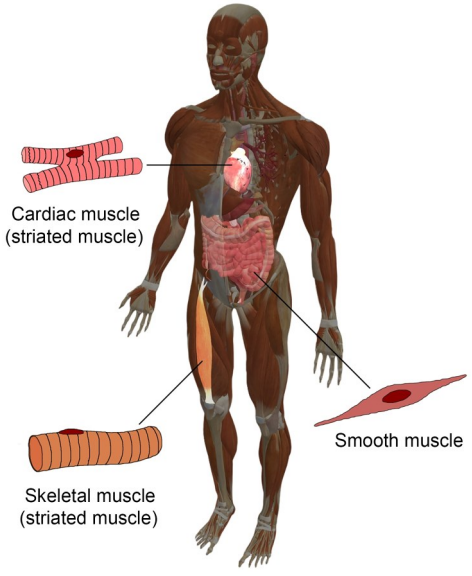

Fig. 1 Three types of human muscle tissues

Compared with smooth muscle, striated muscle has a higher tissue density, larger volume, and stronger load-bearing capacity [30]. This review focuses on the biomechanics analysis of human skeletal muscle.

2.1 Skeletal muscle anatomy

Figure 2a shows the different hierarchical structures of the skeletal muscle, which is composed of many muscle fascicles wrapped in connective tissue. Each muscle fascicle has a cross-sectional area of approximately 1 mm^2, a length of approximately 100 mm, and contains many parallel-aligned muscle fibers. Muscle fibers are roughly 50 μm across. Each muscle fiber is made up of many aligned myofibrils, with the same length as the muscle fascicle. Each myofibril contains more than 50,000 connected basic contractile units, which are referred to as sarcomeres. Each sarcomere comprises two long protein filaments, i.e., actin and myosin, functioning as a molecular motor. Note that a single molecular motor only generates a slight force; however, when molecular motors work together in skeletal muscle, they can output thousands of newtons of force during strong contractions. This complex and precise organizational structure ensures coordinated cooperation between various components, thereby allowing the skeletal muscle to contract and relax effectively.

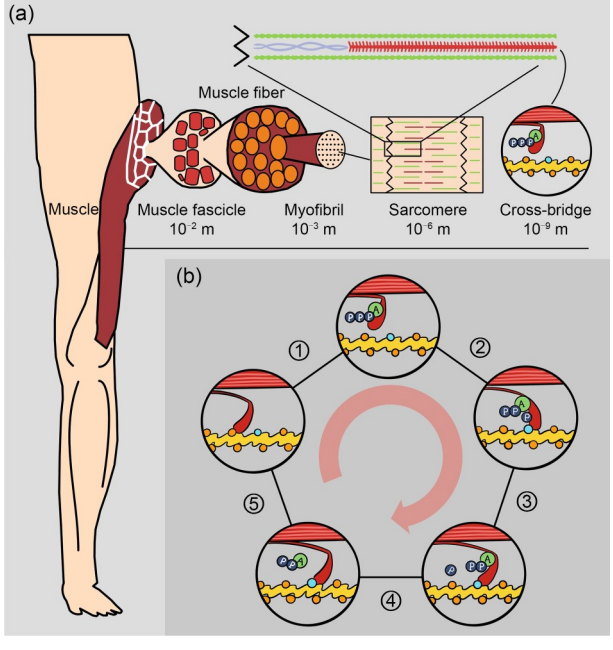

Fig. 2 Anatomy of human skeletal muscle: (a) multi-scale structure of skeletal muscle; (b) the theory of cross-bridge cycle

The cross-bridge cycle is a widely accepted theory to explain the muscle contraction mechanism [31]. As shown in Fig. 2b, myosin can be divided into a head, a neck, and a tail. The head can bind tightly to specific sites on the actin filament (the first phase displayed in Fig. 2b). When the muscle contracts, adenosine triphosphate (ATP) provides energy, which causes the myosin head to detach from one site, swing forward, and bind to the next site (the second and third phases displayed in Fig. 2b). Then, the myosin neck undergoes a twist, pushing the actin filament to slide by 10 nm, thereby generating a force of a few piconewtons. This process is referred to as the power stroke. Then, ATP is decomposed into adenosine diphosphate (ADP), and one phosphorus ion is released from the myosin head (the fourth phase displayed in Fig. 2b). The myosin returns to its initial state (the fifth phase displayed in Fig. 2b). By repeating this cycle continuously, the actin filaments are pulled toward the center of the sarcomere, and this process converts chemical energy into mechanical energy.

2.2 Skeletal muscle morphology

The skeletal muscle exhibits different shapes according to the strength requirements of different body joints. Figure 3a shows three basic types of skeletal muscle shapes, i.e., fusiform, pennate, and strap. Fusiform muscles comprise spindle-shaped muscle fibers with a thicker middle and two narrower ends. For example, the biceps brachii is a fusiform muscle. These muscles are well-suited for rapid and brief movements. Pennate muscles comprise feather-shaped muscle fibers, and they are primarily distributed in the rotational sites of the limbs, the abdominal wall, and the chest wall. Typically, they can provide multiple degrees of freedom and high torque movements, e.g., the gluteus maximus driving abduction/adduction and extension/flexion of the hip joints. The strap muscles comprise band-shaped muscle fibers. They are usually arranged into muscle groups and are distributed in the limbs and torso. For instance, the

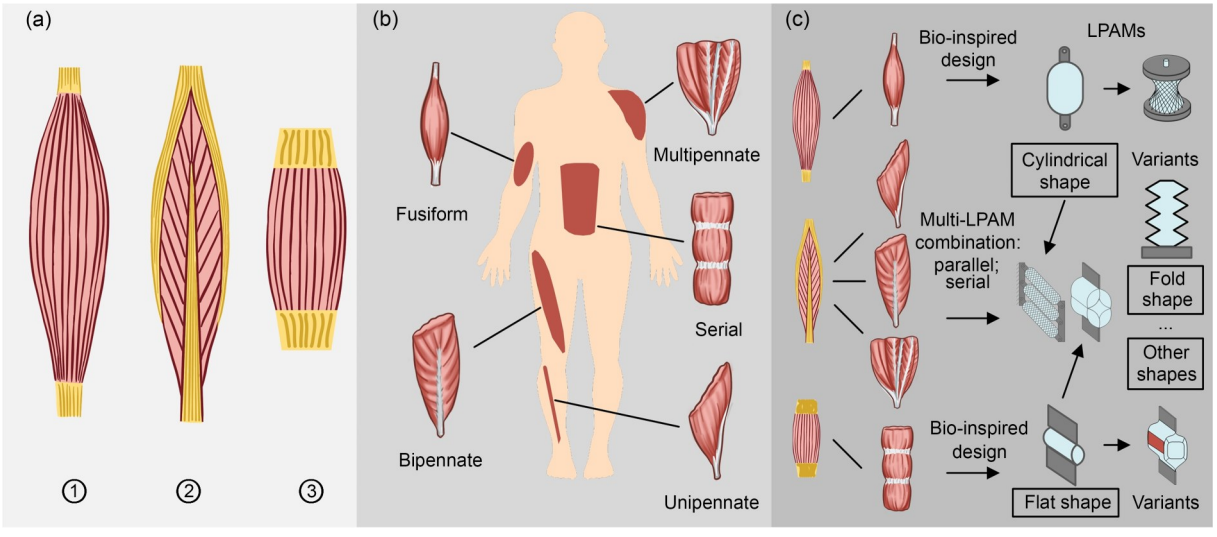

Fig. 3 Fundamental shapes of skeletal muscle: (a) fusiform, pennate, and strap shapes; (b) other shapes (i.e., combinations of these basic shapes); (c) bio-inspired design of LPAMs

rectus abdominis is a muscle group formed by many strap muscles.

In addition to the three basic shapes (fusiform, pennate, and strap), other skeletal muscle shapes are formed through combinations of the basic shapes. As shown in Fig. 3b, the unipennate and multipennate muscles are variations of the pennate muscle, where the former has only half of the pennate structure, and the latter is formed by multiple pennate units connected in parallel. The extensor digitorum longus is a type of unipennate muscle that is long and strong, extending the medial toe joints. The deltoid is a multipennate muscle with significant strength, which enables it to abduct the shoulder joint and assist in lifting heavy objects. The rectus abdominis is a paired muscle, located on either side of the midline of the anterior abdominal wall, and is segmented by tendinous intersections. It is capable of producing a wide range of movements.

As shown in Fig. 3c, the design of LPAMs draws inspiration from the diverse shapes observed in the skeletal muscle. A cylindrical-shaped LPAM is designed to mimic the fusiform muscle, and its variants are developed to improve its mechanical properties, e.g., the contraction ratio, power-weight ratio, and flexibility. A flat-shaped LPAM based on the anatomy and morphology of the strap muscle has also been proposed. This LPAM is completely made of soft materials. Many variants of the flat-shaped LPAM have been developed to promote a high contraction ratio. In addition, drawing inspiration from different pennate muscles, a multi-LPAM combination design has been presented, including parallel, serial, and hybrid modes. A parallel mode is typically adopted to achieve a high output force. Conversely, a serial mode is suitable for achieving a high contraction length. A hybrid mode combines these two advantages. Differing from the abovementioned LPAMs, a fold-shaped muscle, whose structure is not entirely based on a bio-inspired design, is mainly actuated by a negative pressure.

2.3 Skeletal muscle biomechanics

The shapes and arrays of the skeletal muscle inspire the design of LPAMs, and the biomechanical properties of the skeletal muscle, e.g., strain, output force, output energy, and power, can help designers determine the dimensions and objectives of wearable LPAMs. Note that biomechanical properties vary slightly due to individual differences [32]. The muscle actuation strain is about 20%, and the actuation stress of the skeletal muscle is about 0.1 MPa. Table 1 shows the specific metrics.

Table 1 Human skeletal muscle performance metrics from [32]

Metric	Value
Actuation strain	20%
Density	1037 kg/m^3
Actuation stress	0.1 MPa
Efficiency	about 40%
Modulus	10–60 MPa
Specific power	50 W/kg

In LPAM design, the principal technical criteria to be considered include the output force and the contraction length (or the contraction rate). Determining the output force and contraction length based on the different assisted joints is crucial for designers. Herein, we propose the hypothesis that LPAMs can replace skeletal muscle/muscle groups in driving joint movements. Thus, the contraction length and output force of the LPAMs must exceed those of the skeletal muscle associated with the assisted joint.

For example, if the objective is to assist the hip joint in flexion and extension movements, the output force and contraction length of the gluteus maximus and rectus femoris can be referenced. Similarly, if the objective is to aid the knee joint in flexion and extension movements, the quadriceps and hamstring muscles can be considered. In addition, for the ankle joint, the gastrocnemius and plantar flexor muscles can be referenced. The output force and contraction length of these muscles can be obtained using the OpenSim simulation software [33], which provides valuable insights for the design of LPAMs.

OpenSim is an open-source computational platform for simulating [34], analyzing [35], and visualizing the human skeletal muscle system [36], as shown in Figs. 4a and 4b. In this review, we combined data from the study of Arnold et al. [37] to analyze the output force and contraction length of the skeletal muscle in the lower limbs.

In Ref. [37], researchers recruited five healthy participants to walk at speeds of 1.00, 1.25, 1.50, and 1.75 m/s and to run at speeds of 2, 3, 4, and 5 m/s on a treadmill test platform. They measured surface electromyographic signals from 11 different muscles in the lower limbs of the participants and motion data (including angles, angular velocity, and angular acceleration) of the hip, knee, and ankle joints. They then constructed a skeletal muscle model and calculated the parameters of the human skeletal muscles. The maximum output force and the maximum contraction length of the skeletal muscle at the ankle, knee, and hip joints from a subject were extracted (Fig. 4c).

During the walking phase, the soleus muscle exhibits the greatest degree of contraction with a range of 1.9–2.4 cm when the ankle joint is plantarflexed. Notably, the variation in the contraction length is unclear when walking at a speed of 1.00 to 1.75 m/s. During the running phase, when the ankle joint is plantarflexed, the soleus muscle displays the greatest contraction length. In addition, the contraction length decreases with increasing running speed.

During the walking phase, the lateral femoral muscle is responsible for most of the extension movement of the knee joint, with a maximum contraction length of 5.4 cm, and the contraction length increases with increasing walking speed. During the running phase, the lateral femoral muscle contracts by 7.3 cm to facilitate the extension movement of the knee joint at a running speed of 5 m/s.

During the walking phase, the contraction of the rectus femoris muscle is the most obvious when the hip joint is flexed, achieving a maximum contraction distance of 6.8 cm at a walking speed of 1.75 m/s. In addition, during the

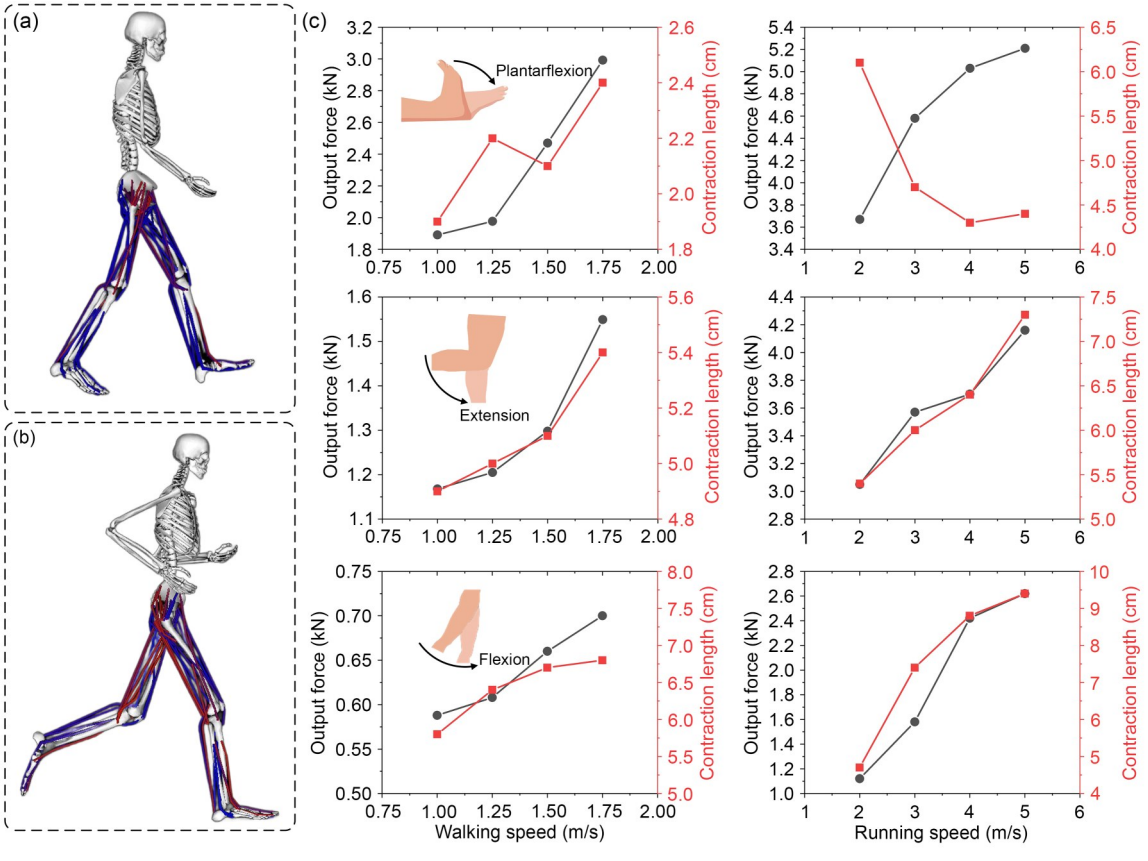

Fig. 4 Simulations and calculated results of musculoskeletal model for human lower limb joints: (a) walking simulation; (b) running simulation; (c) biomechanics of skeletal muscles driving the ankle, knee, and hip joints

running phase, the rectus femoris muscle reaches its maximum contraction length of 9.5 cm at a speed of 5 m/s.

Generally, regardless of whether it is in the walking or running phase, the output force of the crucial skeletal muscles increases with the increasing movement speed of the joints. The maximum force required for ankle movement is 3 kN and 5.2 kN during walking and running. The maximum force at the knee joint is 1.55 kN during walking and 4.15 kN during running. The maximum force at the hip joint is 0.7 kN during walking and 2.6 kN during running.

Overall, the design requirements of LPAMs are determined by the target individuals, assisted human joints, and application scenarios (e.g., level walking [38], rehabilitation training [39], sit-to-stand assisting [40], and uphill walking [41]). In addition, the movements of human joints rely on several corresponding groups of skeletal muscles. Many important biomechanical characteristics of these skeletal muscles, including the contraction force and contraction length, must be calculated in a simulation environment that guides the bio-inspired structural design of LPAMs.

There is an easy-to-understand principle for an LPAM constructed by three key components, i.e., the inner bladder, the outer constricted fabric layer, and the pipe joint. The soft bladder is placed into the enclosed space formed by the constricted fabric layer, and its deformation can be controlled by inputting air pressure. Both ends of the LPAM can contract while compressed air inflates the soft bladder, and then the air pressure energy is converted into mechanical energy. The initial shapes and dimensions of the LPAMs play decisive roles in actuation characterizations. In this review, the LPAMs are classified into cylindrical-shaped muscles [42], flat-shaped muscles [43], fold-shaped muscles [44, 45], and other muscles [46].

3 Linear pneumatic artificial muscles

3.1 Cylindrical-shaped muscles

One of the most common types of cylindrical-shaped muscles is the McKibben muscle, which was the first LPAM [13]. Its conceptual design was proposed by Morin in 1953, and the prototype was fabricated by McKibben using a helically woven structure to create a prosthesis for his daughter, who suffered from polio [47]. Generally, it consists of a rubber inner tube (used as the bladder) surrounded by a woven shell (used as the constricted fabric layer) [48]. When the inner tube is pressurized, both ends of the McKibben muscle produce a contraction force in the axis direction, as shown in Fig. 5a. This contraction force is related to the input air pressure, the contraction length, and the load [49]. To investigate the internal relationship between these factors, an idealized static physical model (Fig. 5b) based on energy conservation was derived by Tondu and Lopez [47]. This model can be expressed as follows:

$$F_{\text{tondu}}=\frac{P'\pi D_0^2}{4}\left[\frac{3}{\tan^2\theta_0}(1-\varepsilon)^2-\frac{1}{\sin^2\theta_0}\right], \quad (1)$$

$$\varepsilon=\frac{L_0-L}{L_0}, 0\le\varepsilon\le\varepsilon_{\max}, \quad (2)$$

where F_{tondu} denotes the contraction force, P' denotes the input air pressure, D_0 denotes the initial diameter of the LPAM, θ_0 denotes the braid angle of the woven shell, L_0 denotes the initial length, L denotes the final length after contraction, and ε denotes the contraction ratio.

Because of the use of soft materials, the McKibben muscle has several advantages, including a high power-weight ratio, low mass or inertia, high mechanical efficiency, and compliance, compared with traditional force-producing mechanisms, e.g., geared motors, hydraulic pistons, and Bowden cables. However, there are some drawbacks, e.g., poor contraction force [50], low contraction ratio [51], stiff muscle body [52], and large hysteresis, thereby causing some difficulties for the initial McKibben muscle to assist human lower limbs accurately in wearable applications [53].

Thus, previous studies have sought design inspirations from the biological mechanisms of human skeletal muscles to promote the actuation characterizations of the McKibben muscle [54–58], as shown in Fig. 5c. The first method involves making some minor changes in the rubber inner tube, woven shell, or contact area between the two parts, targeting a single muscle [59–62]. The second method involves using the same muscles and combining them in parallel, serial, and hybrid manners [63–66], which is inspired by the biological structures of various pennate muscles. The third method is converting the radial expansion of cylindrical-shaped muscles into a contraction movement [67–69], which is inspired by the shape variations of the biceps brachii during contraction and extension.

First, researchers identify ways to improve the structure of the McKibben muscle so that a variety of McKibben variants emerge in an endless stream. To eliminate the hysteresis of LPAMs and the material deformation of the muscle membrane, the first pleated pneumatic artificial muscle (PPAM) was developed by Daerden et al. [70–72], which included a membrane with a high tensile stiffness, as shown in Fig. 5c2. The membrane is uniformly folded together along the long axis and is tightly locked to the fittings (i.e., inlet and outlet ducts) at both ends of the PPAM. When pressurized, the PPAM shortens and begins to bulge. The contraction ratio of the PPAM increases by 40% compared with that of the McKibben muscle, reaching 42%. In

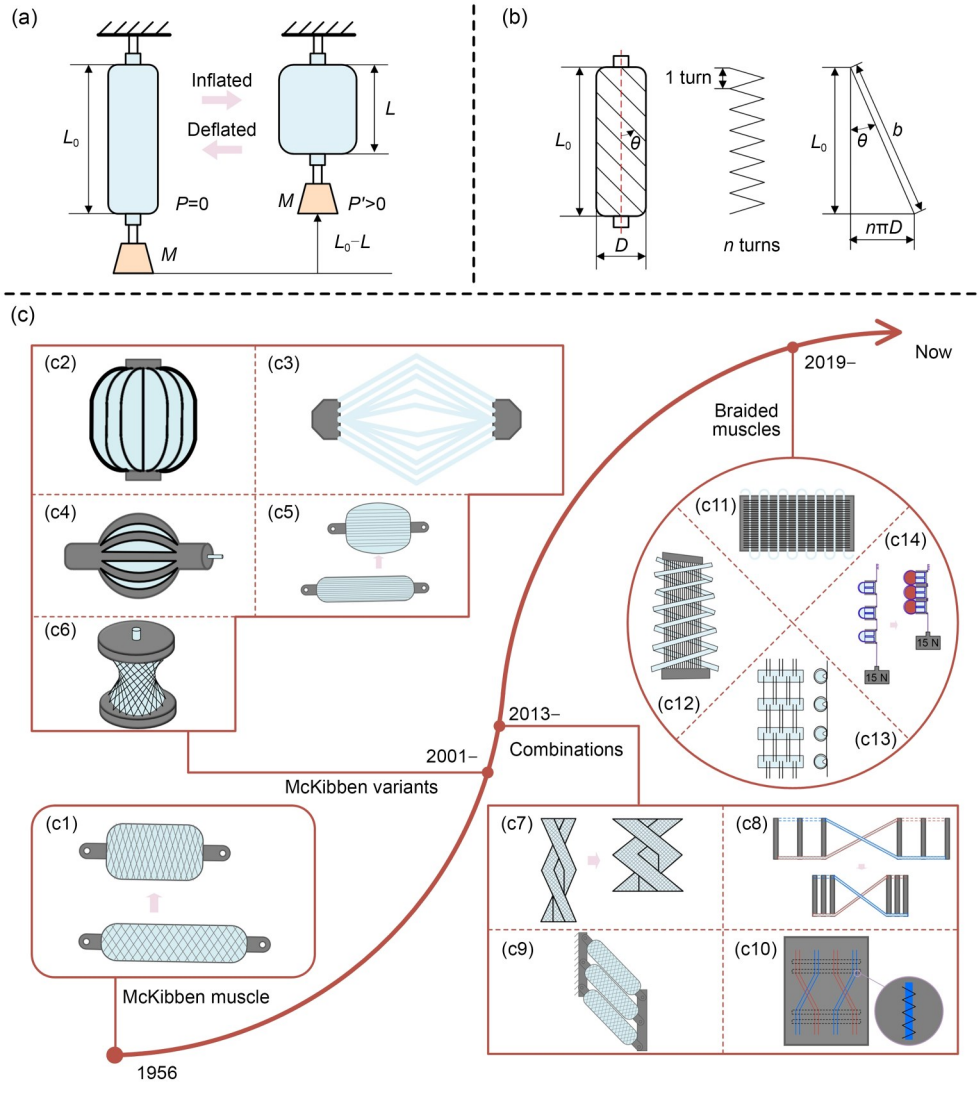

Fig. 5 Cylindrical-shaped LPAMs. (a) Working principle of cylindrical-shaped muscles. (b) Geometric model of McKibben muscle. (c) Various cylindrical-shaped muscles: (c1) McKibben muscle; (c2) pleated pneumatic artificial muscle (PPAM); (c3) thin McKibben muscle; (c4) slit-in-tube actuator; (c5) straight fiber type artificial muscle; (c6) hyperboloidal pneumatic artificial muscle (h-PAM); (c7) active textile-type actuator braided in several strands with thin McKibben muscles; (c8) combined telescopic nested actuator; (c9) McKibben muscle array oriented to mimicking the unipennate muscle; (c10) hook-and-loop fastener actuator with numerous thin McKibben muscles; (c11) active flat textile; (c12) braided flat-tube artificial muscle; (c13) bionic artificial muscle called "ExoMuscle"; (c14) reconfigurable self-sensing pneumatic artificial muscle (RSPAM)

addition, hysteresis is avoided by the folding–unfolding action. A second-generation device was proposed to extend the lifespan of the prototype PPAM [73]. In addition, to promote the production of prototypes, an improved design has been presented [74–76].

To reduce stiffness during contraction, the thinnest McKibben muscle was designed (Fig. 5c3) with a diameter of 1.8 mm, and this design facilitates more flexible deformation compared with the conventional design [77]. Furthermore, a new principle for designing semisoft pneumatic actuators has been reported, and a slit-in-tube actuator for contraction was fabricated [78], as shown in Fig. 5c4. In the slit-in-tube actuator, an elastomeric balloon (used as the inner bladder) is enclosed by an external shell (used as the constricted fabric layer) containing different slits.

To reduce the hysteresis effect, a straight fiber-type artificial muscle has been introduced, which has a specific soft tube [79], where high-strength glass fibers are embedded into the tube. In other words, the bladder and constricted fabric layer are combined into a single element, as shown in Fig. 5c5. As a result, compared with the McKibben muscle, the straight fiber-type artificial muscles exhibit lower hysteresis and a higher contraction ratio. Using straight fibers is an effective method to improve the actuation characterizations of the McKibben muscle; however, the straight fiber-type artificial muscle cannot avoid swelling into a

spherical shape when fully inflated, which restricts bending and limits the applicability of LPAMs in high-flexibility scenarios. Thus, a hyperboloidal pneumatic artificial muscle (h-PAM) was proposed by Watanabe et al. (Fig. 5c6), which can maintain bendability even during contraction [80].

Second, previous studies have developed new pneumatic actuators through different combinations of LPAM units [81, 82], inspired by the biological structures of human skeleton muscle groups (parallel, serial, and forming a cluster). For example, the active textile-type actuator (Fig. 5c7), which is braided in three strands of muscle units, exhibits a maximum contraction ratio of 29.6% at an air pressure of 400 kPa [83]. In addition, its contraction ratio is up to 26.8% greater than that of a single thin muscle. As shown in Fig. 5c8, combined telescopic nested actuators have been developed, and one representative example, i.e., the nested braided actuator [84], effectively doubles the contraction ratio of a single McKibben muscle. However, the contraction force exhibits a 20% to 30% loss compared with the single McKibben muscle.

In addition to bundling muscle units to form a cluster [85], many researchers have investigated connecting McKibben muscles in parallel, mimicking human unipennate muscle with a fundamental feature; i.e., the muscle fibers are uniformly oriented at an angle to the action line. Like muscle fibers, LPAMs expand radially during contraction, which is a critical part of the variable gearing mechanism in unipennate muscles [86]. Thus, the McKibben muscles are arranged in a uniform array at a certain angle (Fig. 5c9), resulting in improved lifting and moving ability (Fig. 5c10).

Third, cylindrical-shaped muscles, represented by McKibben muscles, typically achieve contraction in the axial direction, which means that their flexibility is limited by the stiffness variations of the inflated muscle body. An active flat textile based on a woven structure that can contract in the weft direction has been reported [87]. This contraction is caused by the expansion of thin cylindrical-shaped muscles as warps, as shown in Fig. 5c11. The same design principle is applied to construct a braided flat-tube artificial muscle that yields an output force that is greater than 150 times its weight at an air pressure of 120 kPa (Fig. 5c12) [88]. According to the same design principle, two types of LPAMs were proposed successively by Liu et al. [89, 90], as shown in Figs. 5c13 and 5c14, respectively. One is a bionic artificial muscle, referred to as the "ExoMuscle" [89], which mimics the sarcomere in skeletal muscle with a bio-inspired structure and exhibits a sufficient contraction ratio (50%), an excellent power density (10.94 kW/kg), and remarkable efficiency (69.11%). Note that the performance of the "ExoMuscle" was verified by human subject testing. The other is a reconfigurable self-sensing pneumatic artificial muscle (RSPAM) that can fully satisfy the requirements of safe and friendly interaction with the user [90], including a high contraction ratio, self-contained sensing, reconfiguration, locking capabilities, and no squeezing force.

Although the various cylindrical-shaped muscles can provide sufficient contraction force, high contraction ratio, flexible muscle body, and low hysteresis, researchers continue to explore different shapes for LPAMs to enhance actuation performance.

3.2 Flat-shaped muscles

Flat-shaped muscles [91] represent a novel category of LPAMs, and they are also referred to as pouch motors [92–94] or Peano fluidic muscles [95]. These muscles are distinguished by their square shape, which differs from the tubular configuration observed in the cylindrical-shaped muscles. In addition, they have been investigated for potential use as soft actuators to assist human joint movements [96–100].

A key characteristic of the flat-shaped muscle is its two-dimensional design, which reduces the overall thickness and facilitates simple mechanical structures and easy fabrication [101]. Generally, these muscles are composed of two thin films that are sealed together to form a rectangular cavity. Upon inflation, the center of their rectangular shape uplifts, and both ends of the muscle contract, as shown in Fig. 6a. Here, the contraction force is dependent on the input air pressures, contraction lengths, and loads. The principle of virtual work is employed to establish a relationship between the input air pressure, contraction length, and the load value, as shown in Fig. 6b, and this relation was derived by Niiyama et al. [92] as follows:

$$F_{\text{Niiyama}}(\varphi) = L_0 dP' \frac{\cos\varphi}{\varphi}, \tag{3}$$

$$\varepsilon = \frac{L_0 - L}{L_0} = 1 - \frac{\sin\varphi}{\varphi}, \tag{4}$$

where F_{Niiyama} denotes the contraction force, P' denotes the input air pressure, d denotes the width of the pouch, φ denotes the central angle of the circular segment, L_0 denotes the initial length when the pouch is flat, and L denotes the final length after contraction.

Flat-shaped muscles are primarily made of soft materials, which provide several advantageous properties, e.g., inherent compliance, easy fabrication, and favorable human–robot interaction. However, the contraction ratio is constrained by its structure, reaching only 36.3% in theory according to the geometric model. In experiments, such a contraction ratio is difficult to obtain due to the inability of the longitudinal edges to expand. In addition, the contraction force is constrained by the sealing quality of the rectangular cavity and the burst risk of the thin film. As a result, the

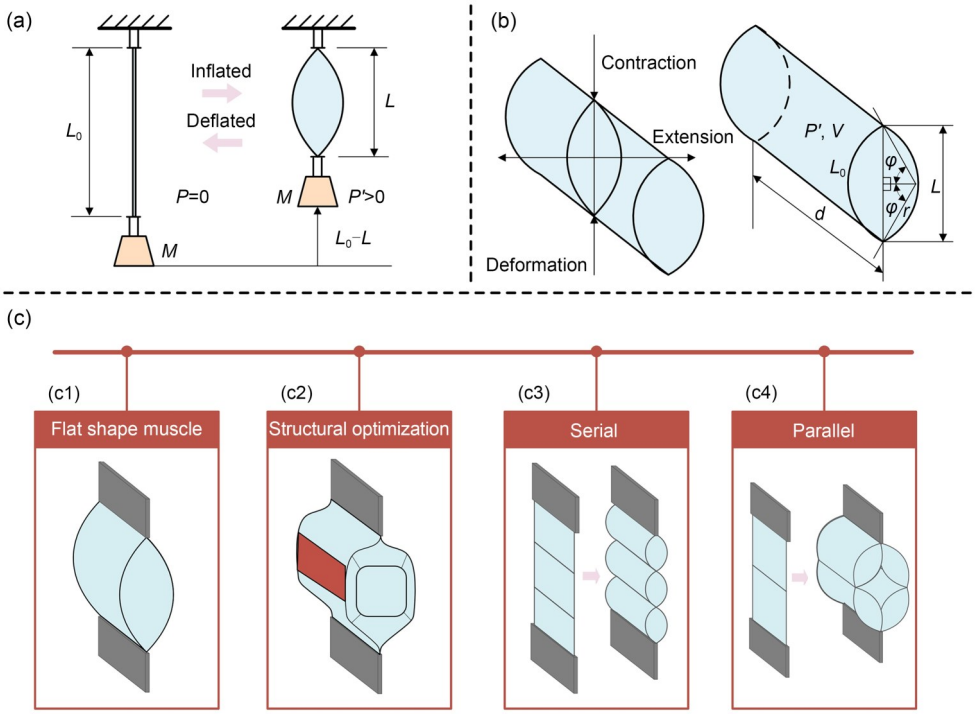

Fig. 6 Flat-shaped LPAMs. (a) Working principle of flat-shaped muscles. (b) Geometric model. (c) Various flat-shaped muscles: (c1) single pouch motor; (c2) structural optimization for single pouch motor; (c3) serial method; (c4) parallel method

original flat-shaped muscle (Fig. 6c1) exhibited a maximum input air pressure of approximately 40 kPa with an output force of 105 N (actuator width: 75 mm) and a maximum contraction ratio of 28% [92].

Drawing inspiration from the biological mechanisms of human skeletal muscles, researchers and engineers have attempted to optimize the structure (Fig. 6c2) or integrate multiple flat-shaped muscle units using serial (Fig. 6c3) and parallel (Fig. 6c4) methods to improve the contraction ratio and contraction force of the flat-shaped muscles.

First, the design of the original flat-shaped muscle unit shape can be optimized by modifying its structure and components [102, 103]. For example, a gusseted pouch motor was developed by introducing a gusset in the pouch [16], thereby removing the limitations caused by the inability of the longitudinal edges to expand. This enabled the actuator to increase its maximum volume such that its output force can increase. The gusseted pouch motor can produce a maximum contraction ratio of 42.6% and output a maximum force of 400 N. In addition, a folded PAM (foldPAM) that features a thin-filmed air pouch folded on each side symmetrically has been proposed [104]. Introducing the folded portion can reduce the limitations caused by the inability of the longitudinal edges to expand when the actuator is inflated. Force–strain relationships can be programmed and tuned by modifying the end geometry, i.e., the width of the laterally folded portion.

Second, flat-shaped muscle units can be integrated using either a parallel [105] or serial [106–109] method, thereby enhancing both the contraction ratio and the contraction force. In addition, the design of paired pouch motors has been proposed [105], and a novel flat-shaped muscle has been developed using parallel methods. The paired pouch motor produces a maximum contraction ratio of 41.9%. Even when the actuator is loaded with a 10-kg weight, the contraction ratio reaches up to 31%. Furthermore, a serial method has been employed to fabricate a long, flat-shaped muscle with three rectangular cavities [107]. Here, three distinct soft materials, including low-density polyethylene, polyester silicone, and fiberglass silicone, were utilized to fabricate the thin films. This actuator, which is constructed from polyester silicone, can withstand an input air pressure of up to 200 kPa, thereby enhancing the contraction force and ratio.

Third, serial and parallel methods are frequently employed to combine flat-shaped muscle units [110], which improves both the contraction ratio and contraction force. A positive pressure-driven X-crossing PAM (X-PAM) has been proposed [15]. Unlike the working principle of conventional pouch motors, the X-PAM directly converts the expansion into linear motion along the actuator axis. A single X-PAM exhibits a contraction ratio of 88.1% when a 1-kg load is suspended. In addition, a serial X-PAM has exhibited a contraction ratio of 88.8% under the same conditions, and an X-PAM with parallel and serial configurations

has demonstrated a contraction ratio of 91% when subjected to a 3-kg load. Thus, the serial and parallel methods have the potential to enhance the actuation characterization of flat-shaped muscles.

In summary, the diversity of flat-shaped muscles offers a multitude of alternatives for bio-inspired LPAMs that have potential use in wearable applications. Flat-shaped muscles can provide a sufficient contraction force, a high contraction ratio, and a soft muscle body; however, the possibility of an actuator burst caused by the positive air pressure is a potential challenge that must be considered. This could hinder the advancement of the flat-shaped muscles.

3.3 Fold-shaped muscles

Fold-shaped LPAMs feature a soft cavity with creases. Typically, fold-shaped muscles are actuated using a vacuum air pressure source, which differs from the methods employed for cylindrical-shaped and flat-shaped muscles. In terms of structural composition, fold-shaped muscles comprise a soft cavity with creases, enclosed ends with rigid parts, and a pipe joint. Typically, fold-shaped muscles can be divided into two primary categories, i.e., bellow-based actuators [111] and Kresling-inspired actuators [112], as shown in Fig. 7. They have been integrated into wearable devices to assist human movements [113, 114], actuated by vacuum or negative air pressure.

Bellow-based actuators consist of a soft outer skin and rigid inner reinforcement parts [115]. This bellow configuration enables fold-shaped muscles to realize a high contraction ratio and a large contraction force, and the reinforcement parts ensure sufficient structural stability during actuation [116, 117]. Their working principle is illustrated in Fig. 7a. Note that bellow-based actuators can extend under positive air pressure and contract under negative air pressure, which enhances their versatility. The contraction ratio and force can be calculated as follows based on the geometric model derived by Joe et al. [115]:

$$\alpha = \sqrt{\frac{2L_0^2}{\pi^2} - \frac{h^2}{4}}, \tag{5}$$

$$F(h) = -P'\left(\frac{\pi D^2}{8} + \frac{\pi h^2}{6} - \frac{\pi}{3}\alpha^2\right), \tag{6}$$

where α denotes the length of the major axis, h denotes the mean pitch, P' denotes the vacuum pressure, D denotes the mean diameter, and F denotes the contraction force.

Compared with positive pressure-driven LPAMs, bellow-based actuators have received considerable attention, and a greater number of variants have been developed [118–120] due to their safety and versatility. A reinforced bidirectional artificial muscle comprising inner and external rings has also been proposed [121], which can contract and extend through the application of positive and negative air

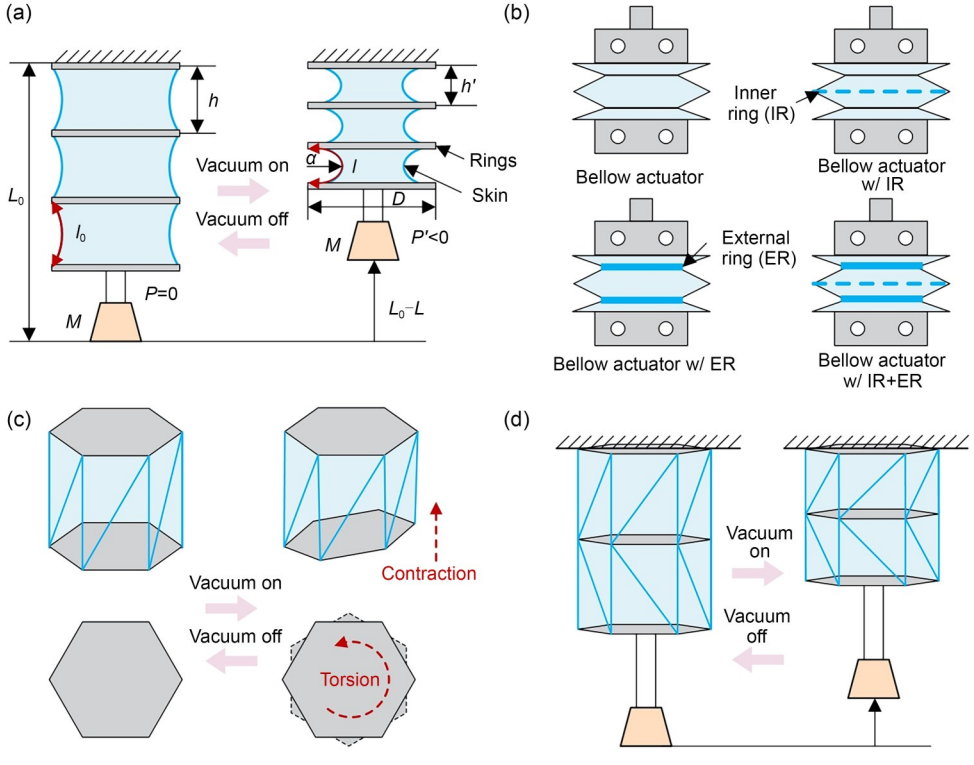

Fig. 7 Fold-shaped LPAMs. (a) Working principle of bellow-type fold-shaped muscles. (b) Variants of bellow-type fold-shaped muscles (w/: with). (c) Vacuum actuator with the Kresling origami structure. (d) Working principle of Kresling-inspired fold-shaped muscles

pressures. Four bellow-based actuators have also been designed to assess the impact of introducing an inner ring (IR) and external ring (ER) on the performance of the actuator, as shown in Fig. 7b. In this review, these are referred to as the bellow actuator, the bellow actuator with IR (w/ IR), the bellow actuator with ER (w/ ER), and the bellow actuator with IR and ER (w/ IR+ER), respectively. Under the same conditions (including the contraction ratio and negative pressure), the bellow actuator with IR and ER exhibits the greatest contraction force. Thus, the addition of further rings to the bellow-based actuator will improve its actuation characteristics.

The Kresling-inspired actuator is another type of fold-shaped muscle. Generally, the actuator is designed using a hybrid method that combines soft and rigid materials [122, 123], and its structure is inspired by Kresling origami, which is derived from the crease pattern of a twisted thin cylinder [124]. The Kresling-inspired actuator can be compressed to a very thin state, which facilitates achieving a high contraction ratio [125, 126]. However, axial contraction/extension and twisting of the Kresling-inspired actuator frequently occur concurrently. As shown in Fig. 7c, this is a soft actuator based on an inclined hexagonal prism structure that deforms along several creases. To achieve pure contraction movement of the Kresling-inspired actuator, two actuation units with opposite tilt directions are spliced, and their cavities are connected, which results in a reduction of the axis length when vacuumed, as shown in Fig. 7d.

Recently, there has been a notable increase in the development of Kresling-inspired actuators. For example, a vacuum-driven Kresling-inspired actuator with low driving pressure, a high contraction ratio, and a fast response was proposed by Liu et al. [127]. This actuator exhibits a contraction ratio of 59% and a response time of 200 ms under a vacuum pressure of 30 kPa. In addition, another Kresling-inspired actuator [128] has been proposed, and this actuator comprises a sealed film chamber that connects the polygonal top and bottom plates with uniformly distributed transverse reinforcements. This actuator can produce a contraction force of 400 N and a contraction ratio of 90%.

3.4 Other muscles

In addition to the three main shapes discussed above, other shapes have been investigated to improve the actuation performance of LPAMs [129–131], simplify the structural design [132], reduce space requirements [133, 134], decrease fabrication cost [135], enhance human–robot interaction [136], and promote adaptability [137, 138]. Specifically, a soft pneumatic helical actuator was proposed by Yuan et al. [139, 140], as shown in Fig. 8a. When pressurized, because the opposing sides of the actuator have different extensibilities, the LPAM contracts and exhibits a helical shape. This actuator has a maximum contraction ratio of 78% at an air pressure of 300 kPa. In addition, to improve the actuation performance of LPAMs, a kirigami mechanism has been employed to design three soft actuators, including parallel kirigami actuators, out-of-plane kirigami actuators, and spiral kirigami actuators [141], as shown in Fig. 8b. Here, parallel kirigami actuators have shown a maximum contraction ratio of up to 78.5% and produce steady forces throughout the motion; thus, they can be applied in scenarios that require large displacements.

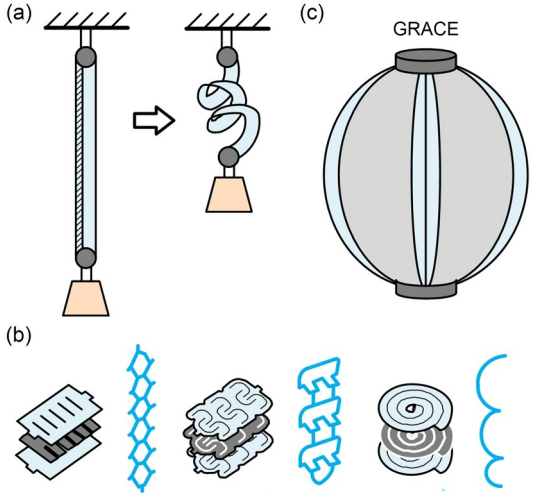

Fig. 8 LPAMs with other shapes. (a) Soft pneumatic helical actuator. (b) Inflatable kirigami actuator. (c) 3D-printed biomimetic artificial muscle

To simplify the structural design of LPAMs, a class of 3D-printed biomimetic artificial muscles, named GeometRy-based Actuators that Contract and Elongate (GRACE), was introduced by De Pascali et al. [132], as shown in Fig. 8c. These devices comprise a single-material pleated membrane, which eliminates the need for strain-limiting elements. These artificial muscles are capable of both contraction and extension, and they can be produced using low-cost additive manufacturing, where the entire structure is printed in full in a single step. Furthermore, a bubble artificial muscle with low fabrication cost has been developed [135], and this artificial muscle is lightweight, flexible, and inexpensive. In addition, the fabrication of these muscles is a relatively straightforward process, where commercial plastic tubing with retaining rings is used to create a "bubble" shape, which forms a series of contractile units that can attain a desired stroke.

Conventional muscle-like soft actuators take up a considerable amount of space, which is a significant limitation when they must be mounted in a limited area. To reduce the space requirements of LPAMs, a small cross-sectional area was designed and realized in a thin-walled actuator that is actuated by vacuum pressures [133]. In addition, a

previous study has presented an artificial pneumatic myofibril with multiple contraction units to form a compact LPAM [134].

To enhance the human–robot interaction of LPAMs, a muscle actuator comprising a series of wedge-like units has been presented and manufactured entirely from silicone rubber. Here, a vacuum-driven mechanism is employed in the actuator that mimics the natural movements of human skeletal muscles. The use of the wedge-like shape, soft silicone rubber materials, and vacuum-driven pneumatic energy facilitates a more lifelike interaction with the human body [136].

To promote the adaptability of LPAMs, a vacuum-driven soft actuator named MORI-A [137] has also been proposed, which enhances the adaptability of LPAMs significantly by introducing a modular deformation structure. This innovation allows for the creation of soft robots with diverse functionalities and forms, thereby overcoming the limitations of traditional LPAMs, which frequently require redesign when different functionalities are needed. In addition, multilayer artificial muscles (MAMs) have been developed [138], representing a notable advancement in adaptability. These MAMs are inspired by the sarcomere and are designed to be compact, versatile, and capable of configurable modularity.

4 Soft wearable robotic system

The McKibben muscle is a representative example of a soft-rigid hybrid LPAM. This classification is attributed to the larger elastic modulus of its bladder and the incorporation of rigid materials at both ends. Nevertheless, the appearance of pouch motors establishes a relationship between LPAMs and soft actuators, resulting from the pouch motors being composed entirely of soft materials. As a result, soft linear actuators, e.g., pouch motors, are referred to as pure soft LPAMs in this review.

Soft wearable robotic systems that employ LPAMs are commonly utilized to assist lower limb joints (i.e., hip [142], knee [143, 144], and ankle [145–147]) across a wide range of scenarios, including level walking, rehabilitation training, sit-to-stand assistance, and uphill walking. However, determining how to integrate LPAMs into soft wearable robotic systems remains an open issue. Generally, there are two principal ways to solve this problem. One method involves affixing the LPAMs directly to the human body using fabric straps, and the other method involves connecting the LPAMs to rigid linkages attached to the human body. Note that muscle-like actuators can be divided into the soft–rigid hybrid LPAM and the pure soft LPAM; thus, as shown in Fig. 9, four binding methods can be employed to form soft wearable robotic systems.

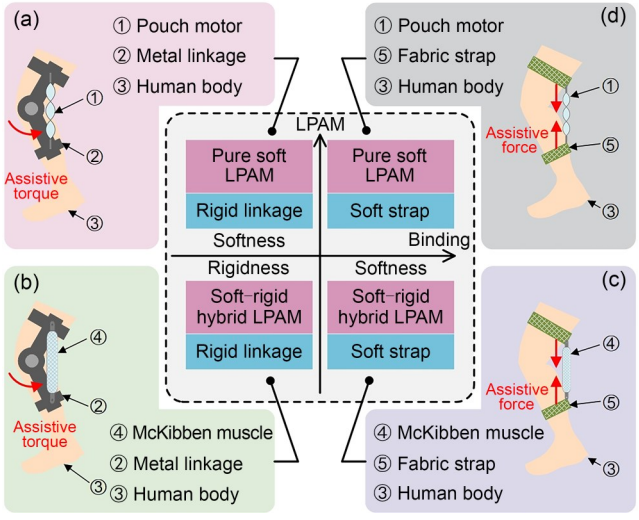

Fig. 9 Binding methods between LPAMs and human bodies. (a) Pure soft LPAMs and rigid linkages. (b) Soft–rigid hybrid LPAMs and rigid linkages. (c) Soft–rigid hybrid LPAMs and soft straps. (d) Pure soft LPAMs and soft straps

A literature review reveals that the first binding method, as shown in Fig. 9a, has not yet been discussed in existing research articles, which may be attributed to the inherent difficulty associated with effectively attaching pure soft LPAMs to rigid linkages.

In the second binding method (Fig. 9b), a high assistive torque provided by the wearable robots can be transmitted and applied to the human joints [148–152]. As shown in Fig. 10a, a powered knee robotic system that employs cylindrical-shaped muscles (i.e., PPAMs) has been developed to achieve the dynamic torques required for zero to full assistance in walking [75].

For the third binding method (Fig. 9c), rigid linkages are replaced by soft straps to connect the cylindrical-shaped muscle and human body, thereby resulting in a change of the power transmission mechanism from assistive torques to assistive forces, which makes it closer to the function of human skeletal muscle [153–164]. As shown in Fig. 10b, a low-pressure cylindrical-shaped muscle has been fabricated using a new customizable process to assist ankle plantarflexion over level walking [147], and its effect was evaluated through surface electromyography.

In the fourth binding method (Fig. 9d), the wearable robotic system is entirely composed of soft materials, which helps reduce its weight and increase its flexibility [165]. For example, a lightweight soft robotic hip exosuit (SR-HExo) based on pouch motors has been proposed [98]. The SR-HExo was used for rehabilitation training of the lower limbs during walking, as shown in Fig. 10c.

The advantages and limitations of the four binding methods are summarized in Table 2. To be specific, the advantages and limitations can be stated as follows:

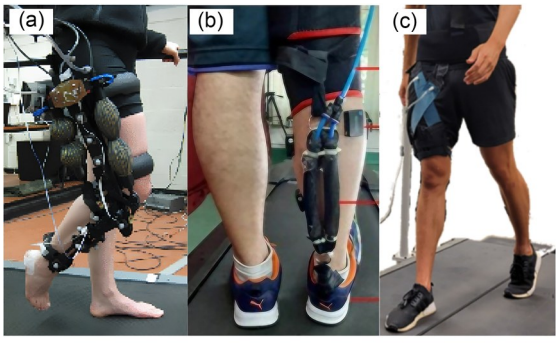

Fig. 10 LPAM-based soft wearable robotic systems for assistance with the human lower limb. (a) Powered knee robotic system with high-dynamic torque. Reproduced from [75], Copyright 2013, with permission from IEEE. (b) Assistive device based on low-pressure LPAM. Reproduced from [147], Copyright 2022, with permission from the Korean Society of Mechanical Engineers and Springer-Verlag GmbH Germany, part of Springer Nature. (c) Lightweight soft wearable robotic system for hip flexion assistance. Reproduced from [98], Copyright 2022, with permission from IEEE

1. For the first binding method, no real application can be found in the extant research literature, which may be due to the difficulty associated with assembly between pure soft LPAMs and rigid linkages.

2. Typically, the second binding method is applied in rehabilitation exoskeletons that can assist individuals with disabilities in performing various activities, e.g., sitting, standing, and walking over level ground. These exoskeletons are always used to assist with hip, knee, or multiple joints due to the advantages of transferring gravity/load to the ground, high energy transfer efficiency, and good control accuracy. However, this method suffers from some limitations, including a bulky structure, poor compliance, and system complexity. Thus, these wearable robotic systems are seldom employed to reduce the metabolic cost of healthy individuals while walking.

3. The third binding method can simplify the robotic structures and reduce the overall weight of the system compared with the second method. Thus, soft wearable robotic systems that utilize this binding method are widely used to provide hip, ankle, and multi-joint assistance, thereby reducing the metabolic cost of healthy users when walking for a long period. In addition, the fourth binding method is used for rehabilitation training.

Soft wearable robotic systems that integrate LPAMs using these four binding methods have been employed in various scenarios [166–168]; however, this review focuses on

Table 2 Comparison of binding methods applied in soft wearable robotic systems

Binding method	Advantage	Limitation	Application scenario	Example	Assisted joint
The first	–	Difficulty in assembly	–	–	–
The second	Transferring gravity/load to the ground; high energy transfer efficiency; high control accuracy	Bulky structure; poor compliance; complex system; interference with physical movement	Level walking	Device [148]	Hip
			Rehabilitation training	Orthosis [152]	Hip
			Sit-to-stand assisting	Assistive suit [143]	Knee
			Sit-to-stand assisting	Exoskeleton [144]	Knee
			Rehabilitation training	KAFO [149]	Multiple joints
			Rehabilitation training	PMs [150]	Multiple joints
The third	Simplified structure; light weight; simple design	Low energy transfer efficiency; slow response	Level walking	pfPAM [156]	Hip
			Level walking	Suit [157]	Hip
			Level walking	AWS [163]	Hip
			Level walking	Device [38]	Ankle
			Rehabilitation training	Ankle-foot orthosis [111]	Ankle
			Uphill walking	Exoskeleton [146]	Ankle
			Level walking	pSTAM [147]	Ankle
			Uphill walking	Exoskeleton [41]	Ankle
			Level walking	Exoskeleton [145]	Ankle
			Uphill walking	Exoskeleton [160]	Ankle
			Level walking	Exosuit [153]	Multiple joints
The fourth	Fitting the human body; easy to wear; comfortable experience; light weight	Low energy transfer efficiency	Sit-to-stand assisting	LPVAc [165]	Hip
			Level walking	SR-HExo [98]	Hip
			Level walking & rehabilitation training	SR-AFO [99]	Ankle

KAFO: knee ankle foot orthosis; PMs: pneumatic muscles; pfPAM: pleated fabric pneumatic artificial muscle; AWS: augmented walking suit; pSTAM: pneumatic silicone tube artificial muscle; LPVAc: low-profile vacuum actuator; SR-HExo: soft robotic hip exosuit; SR-AFO: soft robotic ankle-foot orthosis

assistive devices that can reduce the metabolic cost of users during level walking.

5 Performance comparison

In this review, four main metrics are used to compare the mechanical performance of the LPAMs, i.e., the contraction ratio, maximum force, specific force, and response frequency, which reflect the different mechanical properties of LPAMs. The results of the mechanical properties are shown in Fig. 11. Here, two main metrics are used to exhibit the assistance performance of the LPAM-based wearable robots (Fig. 12). In addition, the advantages and limitations of each type of LPAM in terms of the actuation characteristics and applicability are shown in Table 3.

The cylindrical-shaped muscle response [42] is most closely aligned with the human skeletal muscle (10 Hz), exhibiting a frequency of 6.9 Hz when the actuation stress reaches 400 kPa, as shown in Fig. 11c. In addition, cylindrical-shaped muscles exhibit other advantages, including high stability, precise control, and a high energy-conversion

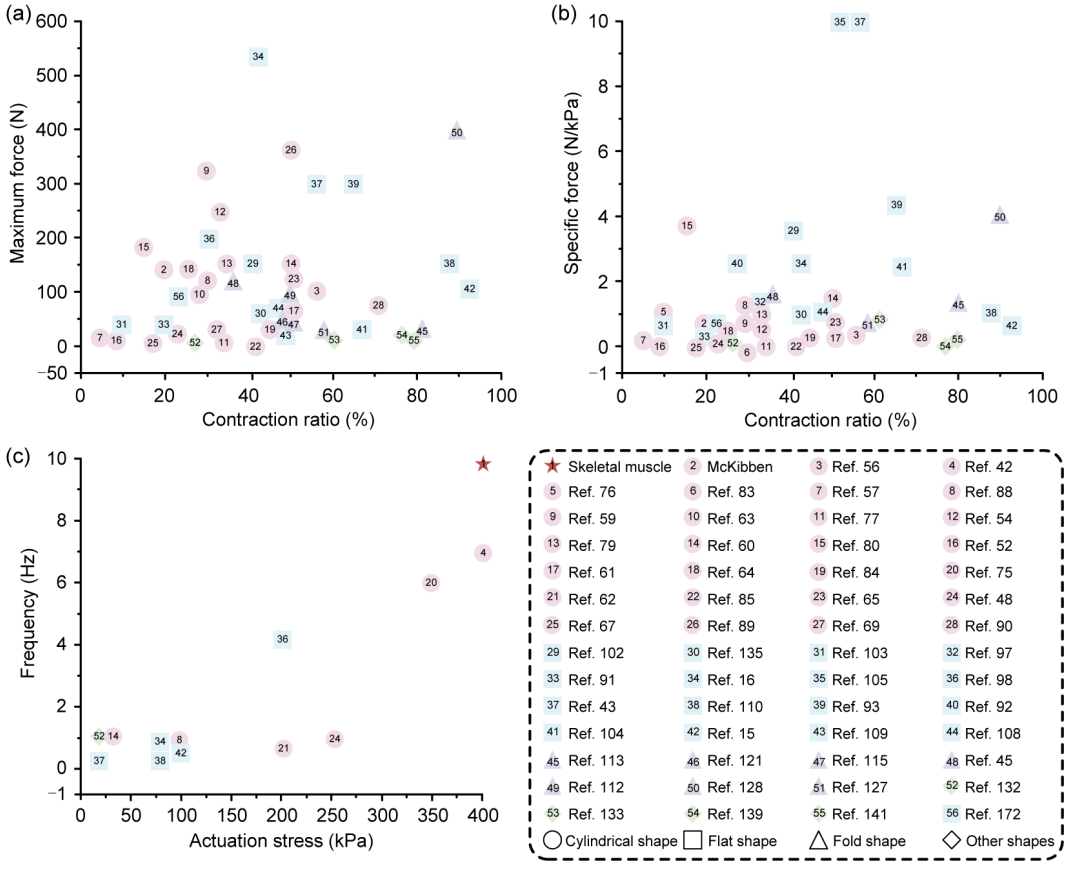

Fig. 11 Comparison of LPAMs. (a) Maximum force versus contraction ratio. (b) Specific force versus contraction ratio. (c) Frequency versus actuation stress

Table 3 Comparison of various types of LPAMs

Shape type	Advantage	Limitation	Human joint	Applicability
Cylindrical	Rapid response; high stability; precise control; high energy-conversion rate	Large actuation stress	Multiple joints	Level walking; uphill walking
Flat	High contraction ratio; soft body; high output force	High hysteresis	Ankle; hip	Rehabilitation training; walking
Fold	High contraction ratio; bidirectional motion	Low fatigue strength	Ankle	Rehabilitation training
Others	Various structures	Fewer wearable applications	–	–

rate. However, their actuation stress (i.e., open pressure) is still large, as shown in Table 3.

The flat-shaped muscle (i.e., the gusseted pouch motor [16]) can produce an output force of up to 526.5 N and exhibit a contraction ratio of 42.6%, as shown in Fig. 11a. In terms of the specific force, two flat-shaped muscles [105, 43] demonstrate noteworthy performance, and they have the same specific force of 10 N/kPa, with contraction ratios of 51.78% and 55.3%, respectively. Another flat-shaped muscle [98] has a response frequency of 4.16 Hz when the actuation stress is equal to 200 kPa. In addition, flat-shaped muscles exhibit favorable human–robot interaction due to the soft body. However, high hysteresis remains a challenge that limits their precise motion control.

The fold-shaped muscle [128] demonstrates a maximum force of 400 N and a contraction ratio of 90% (Fig. 11), and this muscle type can typically perform bidirectional movement. However, its fatigue strength is low, which limits its operational longevity. Other shapes have been utilized in the construction of LPAMs; however, these are seldom utilized in wearable robotics.

Numerous LPAMs have been designed to assist wearers; however, only a few of these devices are utilized in lower limb assistive devices to reduce physical fatigue. For example, cylindrical-shaped muscles have been widely used to assist multiple joints during level walking and uphill walking. Flat-shaped muscles are also typically utilized to assist the ankle and hip joints in rehabilitation training and walking. Conversely, fold-shaped muscles assist ankle rehabilitation training and have the potential to aid other joints.

Specifically, a powered hip exoskeleton [148] can provide an assistive torque of 0.16 N·m/kg at a walking speed of 1 m/s, thereby assisting the hip joint (Fig. 12). It has been demonstrated that this device reduces the net metabolic cost by 13%. In terms of assisting the ankle joint, the exoskeleton [159] can provide 0.3 N·m/kg of assistive torque per bodyweight and reduce the net metabolic cost by 12% at a walking speed of 1.11 m/s. In addition, the assistive robotic device [155] with body-in-the-loop optimization exhibited the greatest reduction in net metabolic cost of 18% at a walking speed of 1.2 m/s. When assisting multiple joints, the knee–ankle–foot exoskeleton [151] reduced the net metabolic cost by 13% when the participants were walking at 1.25 m/s. To reduce the users' metabolic cost during walking, assistive force is generally exerted on the hip and ankle joints.

6 Prospects for next-generation LPAMs

LPAMs have great potential to improve the assistive performance of wearable robots in various fields, such as rehabilitation, prosthetics, and industry assistance, owing to the presence of features like high power-to-weight ratio, flexible movement, lightweight nature, and adaptable compliance. In addition to these advantages, LPAMs possess friendly human–robot interaction as a bionic actuator allowing the wearer's natural range of motion, which is essential for soft wearable robotic systems.

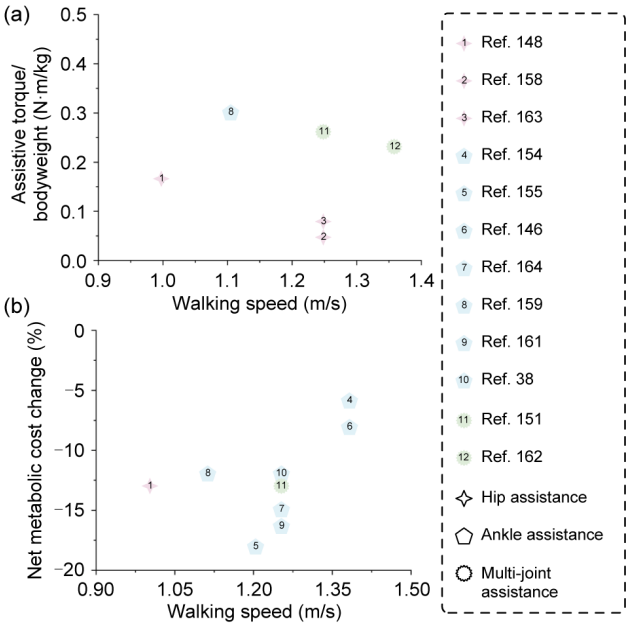

Fig. 12 Comparison of soft wearable robotic systems. (a) Assistive torque/bodyweight versus walking speed. (b) Net metabolic cost versus walking speed

To fabricate high-performance compact soft wearable robots, scientists and engineers propose the use of multifunctional LPAMs. Specifically, in addition to their actuation function, these LPAMs possess a few other capabilities, including variable stiffness, self-sensing capabilities, and untethered actuation. LPAMs are constructed using methods of mechanical designs and functional materials, as shown in Fig. 13.

To integrate variable stiffness into LPAMs, shape memory polymer (SMP) and jamming mechanisms are employed in LPAM-based wearable robots. The SMP is a functional material whose elastic moduli can be altered in response to changes in temperature. For example, helical SMP fibers can be fabricated and utilized as sleeve fibers to constrict cylindrical-shaped muscles, thereby realizing variable contraction characteristics [52]. In addition, jamming mechanisms can be utilized to generate brakes based on friction forces through a vacuum on the layers or particles. Thus, a positive and negative pressure linear brake is incorporated into flat-shaped muscles to regulate the contraction behavior [169]. Furthermore, the antagonistic configuration [143] of two LPAMs across a rotational joint allows LPAM-based wearable robots to exhibit variable stiffness characteristics.

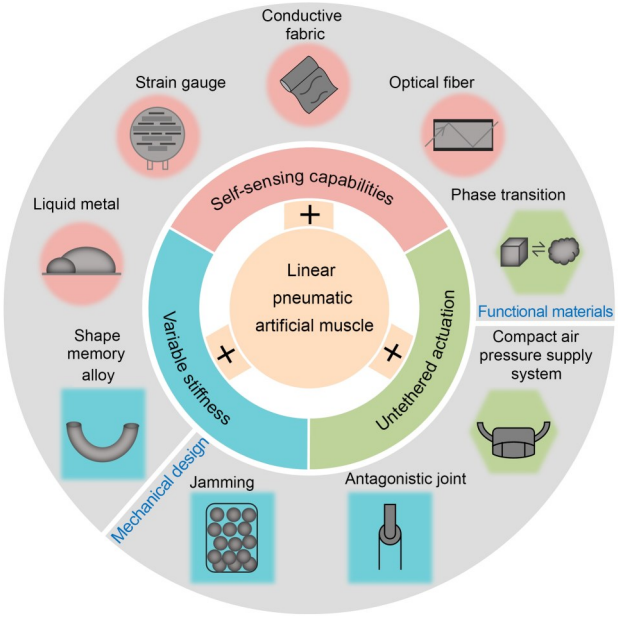

Fig. 13 The next-generation LPAMs for soft wearable robotic systems: LPAMs plus variable stiffness capabilities, LPAMs plus self-sensing mechanisms, and LPAMs plus untethered actuation

The self-sensing capability is a fundamental requirement for LPAM-based wearable robots. To achieve a compact design, various functional materials, including liquid metal [170], strain gauges [171], conductive fabrics [172], and optical fibers [173], are embedded within the LPAMs to capture the kinematic and dynamic data of the actuators such that advanced intelligent control methods can be implemented. A fabric-based soft contractile sensor can be integrated into the flat-shaped muscle structure to measure contraction.

To achieve untethered actuation, it is necessary to combine LPAMs with air supply devices that avoid the utilization of long windpipes. Typically, two methods are employed to achieve this objective. One method involves utilizing the liquid-to-gas phase transition to alter the pressure inside the muscle for mechanical operations [174]. The other method involves the fabrication of a soft pump [175–177] that can be integrated into a portable air pressure supply device. For example, a self-contained soft electrofluidic actuator has been proposed to construct an artificial muscle to stretch a joint. This actuator has demonstrated excellent performance in terms of portability, safety, and actuation [178]. In addition, an external air supply with a compact arrangement has been designed to provide compressed air for the actuator [179].

LPAMs have been investigated for their multifunctional properties in the construction of wearable robots; however, several challenges must be considered in terms of their utilization in real-world applications. First, the reliability of LPAMs is limited by the cycle life, which is a common issue with pressure-driven actuators. Despite the fact that a PAM has achieved more than 10,000 reciprocating cycles [67], the endurance of the device does not satisfy real-world application requirements, and this limitation hinders the widespread promotion and adoption of LPAMs. Second, the efficiency of LPAMs is affected by the energy loss caused by the hysteresis characteristic and the friction between the binding straps and the body. It is difficult for pressure-driven actuators to eliminate the hysteresis characteristic in contraction and extension because of the air compressibility and viscoelastic material properties. Thus, an energy-efficient method is to prevent full expansion and employ a single module [89].

7 Conclusions

This review has discussed and classified various LPAMs that can be utilized to provide assistive force for wearers. The LPAMs are divided into four categories based on their structural shapes, i.e., cylindrical-shaped muscles, flat-shaped muscles, fold-shaped muscles, and other muscles. In addition, several performance metrics are considered to identify which LPAMs have the greatest potential for application in wearable devices, particularly in assisting human lower limb movements (e.g., walking and sit-to-stand assistance).

In addition, this review has summarized LPAM-based soft wearable robotic systems used for metabolic cost reduction during walking. Such devices are frequently employed to aid the hip and ankle joints during level walking at different speeds. Here, the net metabolic cost is employed as a vital metric to assess the assistance performance. Furthermore, when assisting either the hip or the ankle joint, it is evident that the greater the assistive force, the more pronounced the assistance performance.

Acknowledgements This work was supported by the National Natural Science Foundation of China (No. 52475067).

Author contributions ZM and JBL were involved in writing—original draft; ZM investigated the literature and drew the graphs and tables; HTL and TH contributed to writing—review and editing. All authors read and approved the final manuscript for publication.

Declarations

Conflict of interest The authors declare that they have no conflict of interest.

Ethical approval This article does not contain any studies with human or animal subjects performed by any of the authors.

References

1. Raitor M, Ruggles SW, Delp SL et al (2024) Lower-limb exoskeletons appeal to both clinicians and older adults, especially

for fall prevention and joint pain reduction. IEEE Trans Neural Syst Rehabil Eng 32:1577–1585. https://doi.org/ 10.1109/TNSRE.2024.3381979
2. Yoo HJ, Lee J, Cho KJ (2024) Arm back support suit (Abs-Suit) for parcel delivery with a passive load redistribution mechanism. IEEE Robot Autom Lett 9(2):1238–1245. https://doi.org/10.1109/LRA.2023.3340511
3. Kim J, Porciuncula F, Yang HD et al (2024) Soft robotic apparel to avert freezing of gait in Parkinson's disease. Nat Med 30(1): 177–185. https://doi.org/10.1038/s41591-023-02731-8
4. Ma Z, Liu JB, Ma GY et al (2023) Lockable lower-limb exoskeleton based on a novel variable-stiffness joint: reducing physical fatigue at squatting. J Mech Robot 15(5):051008. https://doi.org/10.1115/1.4055964
5. Zhou YM, Hohimer CJ, Young HT et al (2024) A portable inflatable soft wearable robot to assist the shoulder during industrial work. Sci Robot 9(91):eadi2377. https://doi.org/10.1126/scirobotics.adi2377
6. Kim JI, Choi J, Kim J et al (2024) Bilateral back extensor exosuit for multidimensional assistance and prevention of spinal injuries. Sci Robot 9(92):eadk6717. https://doi.org/10.1126/scirobotics.adk6717
7. Hawkes EW, Christensen DL, Okamura AM (2016) Design and implementation of a 300% strain soft artificial muscle. In: IEEE International Conference on Robotics and Automation, p.4022–4029. https://doi.org/10.1109/ICRA.2016.7487592
8. Abe T, Koizumi S, Nabae H et al (2019) Fabrication of "18 weave" muscles and their application to soft power support suit for upper limbs using thin McKibben muscle. IEEE Robot Autom Lett 4(3):2532–2538. https://doi.org/10.1109/LRA.2019.2907433
9. Zhu MJ, Do TN, Hawkes E et al (2020) Fluidic fabric muscle sheets for wearable and soft robotics. Soft Robot 7(2):179–197. https://doi.org/10.1089/soro.2019.0033
10. Bhat A, Jaipurkar SS, Low LT et al (2023) Reconfigurable soft pneumatic actuators using extensible fabric-based skins. Soft Robot 10(5):923–936. https://doi.org/10.1089/soro.2022.0089
11. Schäffer K, Ozkan-Aydin Y, Coad MM (2024) Soft wrist exosuit actuated by fabric pneumatic artificial muscles. IEEE Trans Med Robot Bionics 6(2):718–732. https://doi.org/10.1109/TMRB.2024.3385795
12. Zou J, Feng M, Ding NY et al (2021) Muscle-fiber array inspired, multiple-mode, pneumatic artificial muscles through planar design and one-step rolling fabrication. Natl Sci Rev 8(10): nwab048. https://doi.org/10.1093/nsr/nwab048
13. Chou CP, Hannaford B (1996) Measurement and modeling of McKibben pneumatic artificial muscles. IEEE Trans Robot Autom 12(1):90–102. https://doi.org/10.1109/70.481753
14. Zhu JQ, Chen H, Chai ZP et al (2024) A dual-modal hybrid gripper with wide tunable contact stiffness range and high compliance for adaptive and wide-range grasping objects with diverse fragilities. Soft Robot 11(3):371–381. https://doi.org/10.1089/soro.2023.0022
15. Feng M, Yang DZ, Ren L et al (2023) X-crossing pneumatic artificial muscles. Sci Adv 9(38):eadi7133. https://doi.org/10.1126/sciadv.adi7133
16. Jang JH, Jamil B, Moon Y et al (2023) Design of gusseted pouch motors for improved soft pneumatic actuation. IEEE/ASME Trans Mechatron 28(6):3053–3063. https://doi.org/10.1109/TMECH.2023.3244347
17. Zhang C, Zhu PG, Lin YQ et al (2021) Fluid-driven artificial muscles: bio-design, manufacturing, sensing, control, and applications. Bio-Des Manuf 4(1):123–145. https://doi.org/10.1007/s42242-020-00099-z
18. Grellmann H, Lohse FM, Kamble VG et al (2022) Fundamentals and working mechanisms of artificial muscles with textile application in the loop. Smart Mater Struct 31(2):023001. https://doi.org/10.1088/1361-665X/ac3d9d
19. Higueras-Ruiz DR, Nishikawa K, Feigenbaum H et al (2022) What is an artificial muscle? A comparison of soft actuators to biological muscles. Bioinspir Biomim 17(1):011001. https://doi.org/10.1088/1748-3190/ac3adf
20. Jamil B, Oh N, Lee JY et al (2024) A review and comparison of linear pneumatic artificial muscles. Int J Precis Eng Manuf Green Technol 11(1):277–289. https://doi.org/10.1007/s40684-023-00531-6
21. Al-Mayahi W, Al-Fahaam H (2024) A review of design and modeling of pneumatic artificial muscle. Iraqi J Electr Electron Eng 20(1):122–136. https://doi.org/10.37917/ijeee.20.1.13
22. Kalita B, Leonessa A, Dwivedy SK (2022) A review on the development of pneumatic artificial muscle actuators: force model and application. Actuators 11(10):288. https://doi.org/10.3390/act11100288
23. Tondu B (2012) Modelling of the McKibben artificial muscle: a review. J Intell Mater Syst Struct 23(3):225–253. https://doi.org/10.1177/1045389x11435435
24. Su H, Hou X, Zhang X et al (2022) Pneumatic soft robots: challenges and benefits. Actuators 11(3):92. https://doi.org/10.3390/act11030092
25. Hussain S, Ficuciello F (2024) Advancements in soft wearable robots: a systematic review of actuation mechanisms and physical interfaces. IEEE Trans Med Robot Bionics 6(3):903–929. https://doi.org/ 10.1109/TMRB.2024.3407374
26. Pan M, Yuan CG, Liang XR et al (2022) Soft actuators and robotic devices for rehabilitation and assistance. Adv Intell Syst 4(4):2100140. https://doi.org/10.1002/aisy.202100140
27. Shi YJ, Dong W, Lin WQ et al (2022) Soft wearable robots: development status and technical challenges. Sensors 22(19): 7584. https://doi.org/10.3390/s22197584
28. Gotti C, Sensini A, Zucchelli A et al (2020) Hierarchical fibrous structures for muscle-inspired soft-actuators: a review. Appl Mater Today 20:100772. https://doi.org/10.1016/j.apmt.2020.100772
29. Mukund K, Subramaniam S (2020) Skeletal muscle: a review of molecular structure and function, in health and disease. Wires Syst Biol Med 12(1):e1462. https://doi.org/10.1002/wsbm.1462
30. Rall JA (2018) What makes skeletal muscle striated? Discoveries in the endosarcomeric and exosarcomeric cytoskeleton. Adv Physiol Educ 42(4):672–684. https://doi.org/10.1152/advan.00152.2018
31. Huxley HE (1953) Electron microscope studies of the organisation of the filaments in striated muscle. Biochim Biophys Acta 12(1–2):387–394. https://doi.org/10.1016/0006-3002(53)90156-5
32. Madden JDW, Vandesteeg NA, Anquetil PA et al (2004) Artificial muscle technology: physical principles and naval prospects. IEEE J Ocean Eng 29(3):706–728. https://doi.org/10.1109/JOE.2004.833135
33. Delp SL, Anderson FC, Arnold AS et al (2007) OpenSim: open-source software to create and analyze dynamic simulations of movement. IEEE Trans Biomed Eng 54(11):1940–1950.

https://doi.org/10.1109/TBME.2007.901024
34. Seth A, Hicks JL, Uchida TK et al (2018) OpenSim: simulating musculoskeletal dynamics and neuromuscular control to study human and animal movement. PLoS Comput Biol 14(7): e1006223. https://doi.org/10.1371/journal.pcbi.1006223
35. Lee LF, Umberger BR (2016) Generating optimal control simulations of musculoskeletal movement using OpenSim and MATLAB. PeerJ 4:e1638. https://doi.org/10.7717/peerj.1638
36. De Groote F, Falisse A (2021) Perspective on musculoskeletal modelling and predictive simulations of human movement to assess the neuromechanics of gait. Proc Biol Sci 288(1946): 20202432. https://doi.org/10.1098/rspb.2020.2432
37. Arnold EM, Hamner SR, Seth A et al (2013) How muscle fiber lengths and velocities affect muscle force generation as humans walk and run at different speeds. J Exp Biol 216(Pt 11):2150–2160. https://doi.org/10.1242/jeb.075697
38. Galle S, Malcolm P, Collins SH et al (2017) Reducing the metabolic cost of walking with an ankle exoskeleton: interaction between actuation timing and power. J Neuroeng Rehabil 14(1): 35. https://doi.org/10.1186/s12984-017-0235-0
39. Cao Y, Huang J, Huang ZB et al (2018) Dynamic model of exoskeleton based on pneumatic muscle actuators and experiment verification. In: IEEE-RAS 18th International Conference on Humanoid Robots, p.334–339. https://doi.org/10.1109/HUMANOIDS.2018.8624914
40. Kulasekera AL, Arumathanthri RB, Chathuranga DS et al (2020) A low-profile vacuum actuator: towards a sit-to-stand assist exosuit. In: 3rd IEEE International Conference on Soft Robotics, p.110–115. https://doi.org/10.1109/robosoft48309.2020.9115999
41. Galle S, Malcolm P, Derave W et al (2015) Uphill walking with a simple exoskeleton: plantarflexion assistance leads to proximal adaptations. Gait Posture 41(1):246–251. https://doi.org/10.1016/j.gaitpost.2014.10.015
42. Wang YX, Li YN, Wang JB et al (2024) A novel high-torque bidirectional curl pneumatic muscle with stretchable sheath: design and finite element method analysis. IEEE Robot Autom Mag 31(3):83–96. https://doi.org/10.1109/MRA.2023.3283332
43. Kwon J, Yoon SJ, Park YL (2020) Flat inflatable artificial muscles with large stroke and adjustable force–length relations. IEEE Trans Robot 36(3):743–756. https://doi.org/10.1109/TRO.2019.2961300
44. Felt W, Robertson MA, Paik J (2018) Modeling vacuum bellows soft pneumatic actuators with optimal mechanical performance. In: IEEE International Conference on Soft Robotics, p.534–540. https://doi.org/10.1109/ROBOSOFT.2018.8405381
45. Zaghloul A, Bone GM (2020) 3D shrinking for rapid fabrication of origami-inspired semi-soft pneumatic actuators. IEEE Access 8:191330–191340. https://doi.org/10.1109/ACCESS.2020.3032131
46. Cho HS, Kim TH, Hong TH et al (2020) Ratchet-integrated pneumatic actuator (RIPA): a large-stroke soft linear actuator inspired by sarcomere muscle contraction. Bioinspir Biomim 15(3): 036011. https://doi.org/10.1088/1748-3190/ab7762
47. Tondu B, Lopez P (2000) Modeling and control of McKibben artificial muscle robot actuators. IEEE Control Syst Mag 20(2): 15–38. https://doi.org/10.1109/37.833638
48. Sangian D, Naficy S, Spinks GM et al (2015) The effect of geometry and material properties on the performance of a small hydraulic McKibben muscle system. Sens Actuat A Phys 234: 150–157. https://doi.org/10.1016/j.sna.2015.08.025
49. Krishnan G, Bishop-Moser J, Kim C et al (2015) Kinematics of a generalized class of pneumatic artificial muscles. J Mech Robot 7(4):041014. https://doi.org/10.1115/1.4029705
50. Cullinan MF, Bourke E, Kelly K et al (2017) A McKibben type sleeve pneumatic muscle and integrated mechanism for improved stroke length. J Mech Robot 9(1):011013. https://doi.org/10.1115/1.4035496
51. Yu ZF, Pillsbury T, Wang G et al (2019) Hyperelastic analysis of pneumatic artificial muscle with filament-wound sleeve and coated outer layer. Smart Mater Struct 28(10):105019. https://doi.org/10.1088/1361-665x/ab300d
52. Yahara S, Wakimoto S, Kanda T et al (2019) McKibben artificial muscle realizing variable contraction characteristics using helical shape-memory polymer fibers. Sens Actuat A Phys 295: 637–642. https://doi.org/10.1016/j.sna.2019.06.012
53. Zhou ZC, Kokubu S, Wang YY et al (2022) Optimization of spring constant of a pneumatic artificial muscle-spring driven antagonistic structure. IEEE Robot Autom Lett 7(3):5982–5989. https://doi.org/10.1109/LRA.2022.3162021
54. Zabihollah S, Moezi SA, Sedaghati R (2023) Design optimization of a miniaturized pneumatic artificial muscle and experimental validation. Actuators 12(6):221. https://doi.org/10.3390/act12060221
55. Akashi N, Kuniyoshi Y, Jo T et al (2024) Embedding bifurcations into pneumatic artificial muscle. Adv Sci 11(25):2304402. https://doi.org/10.1002/advs.202304402
56. Zhang XT, Krishnan G (2018) A nested pneumatic muscle arrangement for amplified stroke and force behavior. J Intell Mater Syst Struct 29(6):1139–1156. https://doi.org/10.1177/1045389x17730920
57. Wang YJ, Liu CB, Ren LQ et al (2022) Bioinspired soft actuators with highly ordered skeletal muscle structures. Bio-Des Manuf 5(1):174–188. https://doi.org/10.1007/s42242-021-00148-1
58. Jamil B, Lee S, Choi Y (2019) Fabrication, characterization and control of knit-covered pneumatic artificial muscle. IEEE Access 7:84770–84783. https://doi.org/10.1109/ACCESS.2019.2925682
59. Carvalho ADD, Karanth N, Desai V (2021) Design and characterization of a pneumatic muscle actuator with novel end-fittings for medical assistive applications. Sens Actuat A Phys 331:112877. https://doi.org/10.1016/j.sna.2021.112877
60. Yi J, Chen XJ, Song CY et al (2018) Fiber-reinforced origamic robotic actuator. Soft Robot 5(1):81–92. https://doi.org/10.1089/soro.2016.0079
61. Ball EJ, Meller MA, Chipka JB et al (2016) Modeling and testing of a knitted-sleeve fluidic artificial muscle. Smart Mater Struct 25(11):115024. https://doi.org/10.1088/0964-1726/25/11/115024
62. Kim S, Lee SR, Lee S et al (2022) Power-efficient soft pneumatic actuator using spring-frame collateral compression mechanism. Actuators 11(3):76. https://doi.org/10.3390/act11030076
63. Zhang SX, Gong DX, Yu JJ (2022) Design of a multi-connection pneumatic artificial muscle. In: 12th International Conference on CYBER Technology in Automation, Control,

and Intelligent Systems, p.301–306. https://doi.org/10.1109/CYBER55403.2022.9907615
64. Jenkins T, Bryant M (2020) Pennate actuators: force, contraction and stiffness. Bioinspir Biomim 15(4):046005. https://doi.org/10.1088/1748-3190/ab860f
65. Bruder D, Wood RJ (2022) The chain-link actuator: exploiting the bending stiffness of McKibben artificial muscles to achieve larger contraction ratios. IEEE Robot Autom Lett 7(1):542–548. https://doi.org/10.1109/LRA.2021.3130627
66. Robinson RM, Kothera CS, Wereley NM (2015) Variable recruitment testing of pneumatic artificial muscles for robotic manipulators. IEEE/ASME Trans Mechatron 20(4):1642–1652. https://doi.org/10.1109/TMECH.2014.2341660
67. Xie DS, Zuo SY, Liu JB (2020) A novel flat modular pneumatic artificial muscle. Smart Mater Struct 29(6):065013. https://doi.org/10.1088/1361-665X/ab84b9
68. Xie DS, Liu JB, Kang RJ et al (2021) Fully 3D-printed modular pipe-climbing robot. IEEE Robot Autom Lett 6(2):462–469. https://doi.org/10.1109/LRA.2020.3047795
69. Xie DS, Ma Z, Liu JB et al (2021) Pneumatic artificial muscle based on novel winding method. Actuators 10(5):100. https://doi.org/10.3390/act10050100
70. Daerden F, Lefeber D (2001) The concept and design of pleated pneumatic artificial muscles. Int J Fluid Power 2(3):41–50. https://doi.org/10.1080/14399776.2001.10781119
71. Daerden F, Lefeber D, Verrelst B et al (2001) Pleated pneumatic artificial muscles: actuators for automation and robotics. In: IEEE/ASME International Conference on Advanced Intelligent Mechatronics, p.738–743. https://doi.org/10.1109/AIM.2001.936758
72. Daerden F, Lefeber D, Verrelst B et al (2001) Pleated pneumatic artificial muscles: compliant robotic actuators. In: IEEE/RSJ International Conference on Intelligent Robots and Systems, p.1958–1963. https://doi.org/10.1109/IROS.2001.976360
73. Verrelst B, Van Ham R, Vanderborght B et al (2006) Second generation pleated pneumatic artificial muscle and its robotic applications. Adv Robot 20(7):783–805. https://doi.org/10.1163/156855306777681357
74. Villegas D, Van Damme M, Vanderborght B et al (2012) Third-generation pleated pneumatic artificial muscles for robotic applications: development and comparison with McKibben muscle. Adv Robot 26(11/12):1205–1227. https://doi.org/10.1080/01691864.2012.689722
75. Beyl P, Van Damme M, Ham RV et al (2014) Pleated pneumatic artificial muscle-based actuator system as a torque source for compliant lower limb exoskeletons. IEEE/ASME Trans Mechatron 19(3):1046–1056. https://doi.org/10.1109/TMECH.2013.2268942
76. Terryn S, Brancart J, Lefeber D et al (2018) A pneumatic artificial muscle manufactured out of self-healing polymers that can repair macroscopic damages. IEEE Robot Autom Lett 3(1):16–21. https://doi.org/10.1109/LRA.2017.2724140
77. Kurumaya S, Nabae H, Endo G et al (2017) Design of thin McKibben muscle and multifilament structure. Sens Actuat A Phys 261:66–74. https://doi.org/10.1016/j.sna.2017.04.047
78. Belding L, Baytekin B, Baytekin HT et al (2018) Slit tubes for semisoft pneumatic actuators. Adv Mater 30(9):1704446. https://doi.org/10.1002/adma.201704446
79. Nakamura T (2007) Experimental comparisons between McKibben type artificial muscles and straight fibers type artificial muscles. In: SPIE International Conference on Smart Structures, Devices and Systems, Article 641426. https://doi.org/10.1117/12.698845
80. Watanabe M, Tadakuma K, Tadokoro S (2024) Hyperboloidal pneumatic artificial muscle with braided straight fibers. IEEE Robot Autom Lett 9(5):4242–4249. https://doi.org/10.1109/LRA.2024.3377565
81. Hiramitsu T, Suzumori K, Nabae H et al (2023) Active textile: woven-cloth-like mechanisms consist of thin McKibben actuators. Adv Robot 37(7):480–494. https://doi.org/10.1080/01691864.2022.2156813
82. Nakagawa K, Sakai Y, Funabora Y et al (2022) Turning a functional cloth into an actuator by combining thread-like thin artificial muscles and embroidery techniques. IEEE Robot Autom Lett 7(3):5827–5833. https://doi.org/10.1109/LRA.2022.3157401
83. Kurumaya S, Nabae H, Endo G et al (2019) Active textile braided in three strands with thin McKibben muscle. Soft Robot 6(2): 250–262. https://doi.org/10.1089/soro.2018.0076
84. Kadir MRA, Faudzi AAM, Rahman MAA (2022) Performance evaluation for braided McKibben pneumatic actuators in telescopic nested structure. IEEE Robot Autom Lett 7(4):10906–10913. https://doi.org/10.1109/LRA.2022.3192168
85. Koizumi S, Kurumaya S, Nabae H et al (2020) Recurrent braiding of thin McKibben muscles to overcome their limitation of contraction. Soft Robot 7(2):251–258. https://doi.org/10.1089/soro.2019.0022
86. Azizi E, Roberts TJ (2013) Variable gearing in a biologically inspired pneumatic actuator array. Bioinspir Biomim 8(2):026002. https://doi.org/10.1088/1748-3182/8/2/026002
87. Hiramitsu T, Suzumori K, Nabae H et al (2019) Experimental evaluation of textile mechanisms made of artificial muscles. In: 2nd IEEE International Conference on Soft Robotics, p.1–6. https://doi.org/10.1109/robosoft.2019.8722802
88. Wu CC, Liu H, Lin SY et al (2023) Braiding polythene lay-flat tube into cotton threads for artificial muscle actuation. Adv Intell Syst 5(11):2300428. https://doi.org/10.1002/aisy.202300428
89. Xie DS, Su YJ, Li XL et al (2023) Fluid-driven high-performance bionic artificial muscle with adjustable muscle architecture. Adv Intell Syst 5(6):2200370. https://doi.org/10.1002/aisy.202200370
90. Liu JB, Ma Z, Wang YX et al (2022) Reconfigurable self-sensing pneumatic artificial muscle with locking ability based on modular multi-chamber soft actuator. IEEE Robot Autom Lett 7(4):8635–8642. https://doi.org/10.1109/LRA.2022.3189154
91. Wirekoh J, Park YL (2017) Design of flat pneumatic artificial muscles. Smart Mater Struct 26(3):035009. https://doi.org/10.1088/1361-665X/aa5496
92. Niiyama R, Sun X, Sung C et al (2015) Pouch motors: printable soft actuators integrated with computational design. Soft Robot 2(2):59–70. https://doi.org/10.1089/soro.2014.0023
93. Yang HD, Greczek BT, Asbeck AT (2019) Modeling and analysis of a high-displacement pneumatic artificial muscle with integrated sensing. Front Robot AI 5:136. https://doi.org/10.3389/frobt.2018.00136
94. Yue WC, Bai CX, Lai JW et al (2024) Dual-stroke soft Peltier pouch motor based on pipeless thermo-pneumatic actuation. Adv Eng Mater 26(5):2301408. https://doi.org/10.1002/adem.202301408
95. Sanan S, Lynn PS, Griffith ST (2014) Pneumatic torsional actuators for inflatable robots. J Mech Robot 6(3):031003. https://doi.org/10.1115/1.4026629
96. Natividad RF, Miller-Jackson T, Chen-Hua RY (2021) A

2-DOF shoulder exosuit driven by modular, pneumatic, fabric actuators. IEEE Trans Med Robot Bionics 3(1):166–178. https://doi.org/10.1109/TMRB.2020.3044115
97. Thalman CM, Hsu J, Snyder L et al (2019) Design of a soft ankle-foot orthosis exosuit for foot drop assistance. In: International Conference on Robotics and Automation, p.8436-8442. https://doi.org/10.1109/icra.2019.8794005
98. Baye-Wallace L, Thalman CM, Lee H (2022) Entrainment during human locomotion using a lightweight soft robotic hip exosuit (SR-HExo). IEEE Robot Autom Lett 7(3):6131–6138. https://doi.org/10.1109/LRA.2022.3165225
99. Thalman CM, Debeurre M, Lee H (2021) Entrainment during human locomotion using a soft wearable ankle robot. IEEE Robot Autom Lett 6(3):4265–4272. https://doi.org/10.1109/LRA.2021.3066961
100. Thalman CM, Hertzell T, Debeurre M et al (2022) Multi-degrees-of-freedom soft robotic ankle-foot orthosis for gait assistance and variable ankle support. Wearable Technol 3:e18. https://doi.org/10.1017/wtc.2022.14
101. Park YL, Santos J, Galloway KG et al (2014) A soft wearable robotic device for active knee motions using flat pneumatic artificial muscles. In: IEEE International Conference on Robotics and Automation, p.4805–4810. https://doi.org/10.1109/ICRA.2014.6907562
102. Li SJ, Lin JH, Kang HW et al (2022) Bio-inspired origamic pouch motors with a high contraction ratio and enhanced force output. Robot Auton Syst 149:103983. https://doi.org/10.1016/j.robot.2021.103983
103. Zhou ZX, Ai QS, Meng W et al (2022) Design and finite element modeling of novel flat pneumatic artificial muscles. In: IEEE/ASME International Conference on Advanced Intelligent Mechatronics, p.1341–1346. https://doi.org/10.1109/AIM52237.2022.9863322
104. Wang SC, Frias Miranda E, Blumenschein LH (2023) The folded pneumatic artificial muscle (foldPAM): towards programmability and control via end geometry. IEEE Robot Autom Lett 8(3): 1383–1390. https://doi.org/10.1109/LRA.2023.3238160
105. Oh N, Park YJ, Lee S et al (2019) Design of paired pouch motors for robotic applications. Adv Mater Technol 4(1):1800414. https://doi.org/10.1002/admt.201800414
106. Greer JD, Morimoto TK, Okamura AM et al (2017) Series pneumatic artificial muscles (sPAMs) and application to a soft continuum robot. IEEE Int Conf Robot Autom 2017:5503–5510. https://doi.org/10.1109/ICRA.2017.7989648
107. Veale AJ, Xie SQ, Anderson IA (2016) Modeling the Peano fluidic muscle and the effects of its material properties on its static and dynamic behavior. Smart Mater Struct 25(6):065014. https://doi.org/10.1088/0964-1726/25/6/065014
108. Xie DS, Liu JB, Zuo SY (2021) Pneumatic artificial muscle with large stroke based on a contraction ratio amplification mechanism and self-contained sensing. IEEE Robot Autom Lett 6(4):8599–8606. https://doi.org/10.1109/LRA.2021.3113375
109. Wang YX, Ma Z, Zuo SY et al (2023) A novel wearable pouch-type pneumatic artificial muscle with contraction and force sensing. Sens Actuat A Phys 359:114506. https://doi.org/10.1016/j.sna.2023.114506
110. Yang DZ, Feng M, Gu GY (2024) High-stroke, high-output-force, fabric-lattice artificial muscles for soft robots. Adv Mater 36(2):2306928. https://doi.org/10.1002/adma.202306928
111. Heung KH, Lei T, Liang KX et al (2024) Quasi-static modeling framework for soft bellow-based biomimetic actuators. Biomimetics 9(3):160. https://doi.org/10.3390/biomimetics9030160
112. Zhang Z, Fan WC, Chen GL et al (2021) A 3D printable origami vacuum pneumatic artificial muscle with fast and powerful motion. In: IEEE 4th International Conference on Soft Robotics, p.551–554. https://doi.org/10.1109/robosoft51838.2021.9479194
113. Gollob SD, Mendoza MJ, Koo BHB et al (2023) A length-adjustable vacuum-powered artificial muscle for wearable physiotherapy assistance in infants. Front Robot AI 10: 1190387. https://doi.org/10.3389/frobt.2023.1190387
114. Park J, Choi J, Kim SJ et al (2020) Design of an inflatable wrinkle actuator with fast inflation/deflation responses for wearable suits. IEEE Robot Autom Lett 5(3):3799–3805. https://doi.org/10.1109/LRA.2020.2976299
115. Joe S, Totaro M, Wang HB et al (2021) Development of the ultralight hybrid pneumatic artificial muscle: modelling and optimization. PLoS ONE 16(4):e0250325. https://doi.org/10.1371/journal.pone.0250325
116. Wang T, Zhu JW, Li F et al (2024) Development of negative-pressure artificial muscles with fiber constraints and pre-stretched soft skin. IEEE Robot Autom Lett 9(1):414–419. https://doi.org/10.1109/LRA.2023.3333704
117. Wang T, Wang X, Fu GQ et al (2024) Theoretical study of vacuum-powered artificial muscles with inner support and flexible skin. Eng Res Express 6(2):025201. https://doi.org/10.1088/2631-8695/ad3716
118. Wu Z, Zhao P, Lei J (2024) Analyzing the contraction force of artificial muscles under negative pressure actuation. Exp Tech 48(4):693–707. https://doi.org/10.1007/s40799-023-00686-6
119. Gregov G, Ploh T, Kamenar E (2022) Design, development and experimental assessment of a cost-effective bellow pneumatic actuator. Actuators 11(6):170. https://doi.org/10.3390/act11060170
120. Coutinho A, Rodrigue H (2023) Fluidic hardware strategies for powering combined negative- and positive-pressure artificial muscles. Adv Eng Mater 25(14):2300071. https://doi.org/10.1002/adem.202300071
121. Coutinho A, Kim S, Rodrigue H (2024) Reinforced bidirectional artificial muscles: enhancing force and stability for soft robotics. Intell Serv Robot 17(1):55–66. https://doi.org/10.1007/s11370-023-00487-1
122. Mendoza MJ, Cancán S, Surichaqui S et al (2024) Versatile vacuum-powered artificial muscles through replaceable external reinforcements. Front Robot AI 10:1289074. https://doi.org/10.3389/frobt.2023.1289074
123. Lee JY, Rodrigue H (2019) Efficiency of origami-based vacuum pneumatic artificial muscle for off-grid operation. Int J Precis Eng Manuf Green Technol 6(4):789–797. https://doi.org/10.1007/s40684-019-00142-0
124. Zang SX, Misseroni D, Zhao T et al (2024) Kresling origami mechanics explained: experiments and theory. J Mech Phys Solids 188:105630. https://doi.org/10.1016/j.jmps.2024.105630
125. Jin T, Li L, Wang TH et al (2022) Origami-inspired soft actuators for stimulus perception and crawling robot applications. IEEE Trans Robot 38(2):748–764. https://doi.org/10.1109/TRO.2021.3096644
126. Jiao ZD, Zhang C, Ruan JP et al (2021) Re-foldable origami-inspired bidirectional twisting of artificial muscles reproduces biological motion. Cell Rep Phys Sci 2(5):100407. https://doi.org/10.1016/j.xcrp.2021.100407
127. Liu JB, Ma GY, Ma Z et al (2023) Origami-inspired soft-rigid hybrid contraction actuator and its application in pipe-crawling

robot. Smart Mater Struct 32(6):065015. https://doi.org/10.1088/1361-665X/acd0e7
128. Lee JY, Rodrigue H (2019) Origami-based vacuum pneumatic artificial muscles with large contraction ratios. Soft Robot 6(1): 109–117. https://doi.org/10.1089/soro.2018.0063
129. Chen FF, Miao YP, Zhang L et al (2022) Triply periodic channels enable soft pneumatic linear actuator with single material and scalability. IEEE Robot Autom Lett 7(2):2668–2675. https://doi.org/10.1109/LRA.2022.3143292
130. Han K, Kim NH, Shin D (2018) A novel soft pneumatic artificial muscle with high-contraction ratio. Soft Robot 5(5):554 – 566. https://doi.org/10.1089/soro.2017.0114
131. Yang D, Verma MS, So JH et al (2016) Buckling pneumatic linear actuators inspired by muscle. Adv Mater Technol 1(3): 1600055. https://doi.org/10.1002/admt.201600055
132. De Pascali C, Naselli GA, Palagi S et al (2022) 3D-printed biomimetic artificial muscles using soft actuators that contract and elongate. Sci Robot 7(68):eabn4155. https://doi.org/10.1126/scirobotics.abn4155
133. Kulasekera AL, Arumathanthri RB, Chathuranga DS et al (2021) A thin-walled vacuum actuator (ThinVAc) and the development of multi-filament actuators for soft robotic applications. Sens Actuat A Phys 332:113088. https://doi.org/10.1016/j.sna.2021.113088
134. Labazanova L, Wu ZY, Gu ZP et al (2021) Bio-inspired design of artificial striated muscles composed of sarcomere-like contraction units. In: 20th International Conference on Advanced Robotics, p.370–377. https://doi.org/10.1109/icar53236.2021.9659330
135. Diteesawat RS, Helps T, Taghavi M et al (2021) Characteristic analysis and design optimization of bubble artificial muscles. Soft Robot 8(2):186–199. https://doi.org/10.1089/soro.2019.0157
136. Oguntosin V, Akindele A (2019) Design and characterization of artificial muscles from wedge-like pneumatic soft modules. Sens Actuat A Phys 297:111523. https://doi.org/10.1016/j.sna.2019.07.047
137. Ogawa J, Mori T, Watanabe Y et al (2022) MORI-A: soft vacuum-actuated module with 3D-printable deformation structure. IEEE Robot Autom Lett 7(2):2495–2502.
138. Ambrose JW, Tan GYE, Chiang NZR et al (2023) Sarcomere-inspired multilayer artificial muscle units for hyperconfigurable robotic applications. Adv Intell Syst 5(12):2300410. https://doi.org/10.1002/aisy.202300410
139. Yuan PZ, Kawano G, Tsukagoshi H (2020) Design and modeling of soft pneumatic helical actuator with high contraction ratio. J Robot Mechatron 32(5):1061–1070. https://doi.org/10.20965/jrm.2020.p1061
140. Yuan PZ, Kawano G, Tsukagoshi H (2019) Soft pneumatic helical actuator with high contraction ratio. In: IEEE/RSJ International Conference on Intelligent Robots and Systems, p.8300-8305. https://doi.org/10.1109/iros40897.2019.8968281
141. Chung S, Coutinho A, Rodrigue H (2023) Manufacturing and design of inflatable kirigami actuators. IEEE Robot Autom Lett 8(1):25–32. https://doi.org/10.1109/LRA.2022.3221318
142. Kawamura T, Takanaka K, Nakamura T et al (2013) Development of an orthosis for walking assistance using pneumatic artificial muscle: a quantitative assessment of the effect of assistance. In: IEEE 13th International Conference on Rehabilitation Robotics, p.1–6. https://doi.org/10.1109/ICORR.2013.6650350
143. Kimura S, Suzuki R, Machida K et al (2021) Development of an exoskeleton-type assist suit utilizing variable stiffness control devices based on human joint characteristics. Actuators 10(1): 17. https://doi.org/10.3390/act10010017
144. Furukawa JI, Okajima S, An Q et al (2022) Selective assist strategy by using lightweight carbon frame exoskeleton robot. IEEE Robot Autom Lett 7(2):3890–3897. https://doi.org/10.1109/LRA.2022.3148799
145. Antonellis P, Galle S, De Clercq D et al (2018) Altering gait variability with an ankle exoskeleton. PLoS ONE 13(10): e0205088. https://doi.org/10.1371/journal.pone.0205088
146. Galle S, Malcolm P, Derave W et al (2014) Enhancing performance during inclined loaded walking with a powered ankle-foot exoskeleton. Eur J Appl Physiol 114(11):2341–2351. https://doi.org/10.1007/s00421-014-2955-1
147. Arora A, Sarkar D, Kumar A et al (2022) Low-pressure pneumatic muscles: development, phenomenological modeling, and evaluation in assistive applications through sEMG analysis. J Mech Sci Technol 36(9):4719–4733. https://doi.org/10.1007/s12206-022-0832-0
148. Young AJ, Gannon H, Ferris DP (2017) A biomechanical comparison of proportional electromyography control to biological torque control using a powered hip exoskeleton. Front Bioeng Biotechnol 5:37. https://doi.org/10.3389/fbioe.2017.00037
149. Teng CM, Wong Z, Teh W et al (2012) Design and development of inexpensive pneumatically-powered assisted knee-ankle-foot orthosis for gait rehabilitation-preliminary finding. In: International Conference on Biomedical Engineering, p.28–32. https://doi.org/10.1109/ICoBE.2012.6178949
150. Zhang MS, Huang J, Cao Y et al (2022) Echo state network-enhanced super-twisting control of passive gait training exoskeleton driven by pneumatic muscles. IEEE/ASME Trans Mechatron 27(6):5107–5118. https://doi.org/10.1109/TMECH.2022.3172715
151. Malcolm P, Galle S, Derave W et al (2018) Bi-articular knee-ankle-foot exoskeleton produces higher metabolic cost reduction than weight-matched mono-articular exoskeleton. Front Neurosci 12:69. https://doi.org/10.3389/fnins.2018.00069
152. Do Nascimento BG, Santos Vimieiro CB, Nagem DAP et al (2008) Hip orthosis powered by pneumatic artificial muscle: voluntary activation in absence of myoelectrical signal. Artif Organs 32(4):317–322. https://doi.org/10.1111/j.1525-1594.2008.00549.x
153. Wehner M, Quinlivan B, Aubin PM et al (2013) A lightweight soft exosuit for gait assistance. In: IEEE International Conference on Robotics and Automation, p.3362–3369. https://doi.org/10.1109/ICRA.2013.6631046
154. Malcolm P, Derave W, Galle S et al (2013) A simple exoskeleton that assists plantarflexion can reduce the metabolic cost of human walking. PLoS ONE 8(2):e56137. https://doi.org/10.1371/journal.pone.0056137
155. Koller JR, Gates DH, Ferris DP et al (2016) 'Body-in-the-loop' optimization of assistive robotic devices: a validation study. In: Proceedings of Robotics: Science and Systems, p.1–10. https://doi.org/10.15607/rss.2016.xii.007
156. Banyarani PB, Tarvirdizadeh B, Hadi A (2024) Design and fabrication of a soft wearable robot using a novel pleated fabric pneumatic artificial muscle (pfPAM) to assist walking. Sens Actuat A Phys 370:115278.

https://doi.org/10.1016/j.sna.2024.115278
157. Kawamura T, Noma M, Nakamura T (2014) Development of a passive switching cam mechanism for walking assistance using pneumatic artificial muscle. In: IEEE/ASME International Conference on Advanced Intelligent Mechatronics, p.1486–1491. https://doi.org/10.1109/AIM.2014.6878293
158. Ogawa K, Thakur C, Ikeda T et al (2017) Development of a pneumatic artificial muscle driven by low pressure and its application to the unplugged powered suit. Adv Robot 31(21): 1135–1143. https://doi.org/10.1080/01691864.2017.1392345
159. Galle S, Derave W, Bossuyt F et al (2017) Exoskeleton plantarflexion assistance for elderly. Gait Posture 52:183–188. https://doi.org/10.1016/j.gaitpost.2016.11.040
160. Sawicki GS, Ferris DP (2009) Mechanics and energetics of incline walking with robotic ankle exoskeletons. J Exp Biol 212(1):32–41. https://doi.org/10.1242/jeb.017277
161. Sawicki GS, Ferris DP (2008) Mechanics and energetics of level walking with powered ankle exoskeletons. J Exp Biol 211(9): 1402–1413. https://doi.org/10.1242/jeb.009241
162. Miyazaki T, Kawase T, Kanno T et al (2021) Running motion assistance using a soft gait-assistive suit and its experimental validation. IEEE Access 9:94700–94713.
163. Thakur C, Ogawa K, Tsuji T et al (2018) Soft wearable augmented walking suit with pneumatic gel muscles and stance phase detection system to assist gait. IEEE Robot Autom Lett 3(4):4257–4264. https://doi.org/10.1109/LRA.2018.2864355
164. Malcolm P, Galle S, Van den Berghe P et al (2018) Exoskeleton assistance symmetry matters: unilateral assistance reduces metabolic cost, but relatively less than bilateral assistance. J Neuroeng Rehabil 15(1):74. https://doi.org/10.1186/s12984-018-0381-z
165. Kulasekera AL, Arumathanthri RB, Chathuranga DS et al (2021) A low-profile vacuum actuator (LPVAc) with integrated inductive displacement sensing for a novel sit-to-stand assist exosuit. IEEE Access 9:117067–117079.
166. Furukawa JI, Noda T, Teramae T et al (2016) An EMG-driven weight support system with pneumatic artificial muscles. IEEE Syst J 10(3):1026–1034. https://doi.org/10.1109/JSYST.2014.2330376
167. Hong JC, Fukushima Y, Suzuki S et al (2017) Estimation of ankle dorsiflexion torque during loading response phase for spring coefficient identification. In: IEEE International Conference on Robotics and Biomimetics, p.2237–2242. https://doi.org/10.1109/ROBIO.2017.8324751
168. Pulvirenti E, Diteesawat RS, Hauser H et al (2022) Towards a soft exosuit for hypogravity adaptation: design and control of lightweight bubble artificial muscles. In: IEEE 5th International Conference on Soft Robotics, p.651–656. https://doi.org/10.1109/RoboSoft54090.2022.9762121
169. Jang JH, Coutinho A, Park YJ et al (2023) A positive and negative pressure soft linear brake for wearable applications. IEEE Trans Ind Electron 70(1):688–698. https://doi.org/10.1109/TIE.2022.3148746
170. Zhong SY, Gai ZY, Yang Y et al (2022) A contraction length feedback method for the McKibben pneumatic artificial muscle. Sens Actuat A Phys 334:113321. https://doi.org/10.1016/j.sna.2021.113321
171. Saga N, Shimada K, Inamori D et al (2022) Smart pneumatic artificial muscle using a bend sensor like a human muscle with a muscle spindle. Sensors 22(22):8975. https://doi.org/10.3390/s22228975
172. Kim W, Park H, Kim J (2021) Compact flat fabric pneumatic artificial muscle (ffPAM) for soft wearable robotic devices. IEEE Robot Autom Lett 6(2):2603–2610. https://doi.org/10.1109/LRA.2021.3062012
173. Tian WH, Wakimoto S, Yamaguchi D et al (2024) Development of a smart artificial muscle using optical fibres. Smart Mater Struct 33(5):055047. https://doi.org/10.1088/1361-665X/ad3ec9
174. Mirvakili SM, Sim D, Hunter IW et al (2020) Actuation of untethered pneumatic artificial muscles and soft robots using magnetically induced liquid-to-gas phase transitions. Sci Robot 5(41):eaaz4239. https://doi.org/10.1126/scirobotics.aaz4239
175. Tang W, Zhang C, Zhong YD et al (2021) Customizing a self-healing soft pump for robot. Nat Commun 12(1):2247. https://doi.org/10.1038/s41467-021-22391-x
176. Guo XY, Tang W, Qin KC et al (2024) Powerful UAV manipulation via bioinspired self-adaptive soft self-contained gripper. Sci Adv 10(19):eadn6642. https://doi.org/10.1126/sciadv.adn6642
177. Tang W, Zhong YD, Xu HX et al (2023) Self-protection soft fluidic robots with rapid large-area self-healing capabilities. Nat Commun 14(1):6430. https://doi.org/10.1038/s41467-023-42214-5
178. Tang W, Lin YQ, Zhang C et al (2021) Self-contained soft electrofluidic actuators. Sci Adv 7(34):eabf8080. https://doi.org/10.1126/sciadv.abf8080
179. Ide M, Hashimoto T, Matsumoto K et al (2020) Evaluation of the power assist effect of muscle suit for lower back support. IEEE Access 9:3249–3260. https://doi.org/10.1109/ACCESS.2020.3047637